

## RESEARCH ARTICLE

# Improved ADI Iterative Algorithm With Gauss-Seidel Ideology for Efficient WLP-FDTD Method in 3-D Cylindrical Coordinate System

DA-WEI ZHU<sup>1,2</sup>, HAI-LIN CHEN<sup>2</sup>, JIACHEN XU<sup>1,3</sup>, BO-AO XU<sup>4</sup>, AND LI ZHEN<sup>1</sup><sup>1</sup>College of Electrical Engineering, Nanjing Vocational University of Industry Technology, Nanjing 210023, China<sup>2</sup>National Key Laboratory on Electromagnetic Environmental Effects and Electro-Optical Engineering, PLA Army Engineering University, Nanjing 210007, China<sup>3</sup>College of Mechanical and Electrical Engineering, Nanjing University of Aeronautics and Astronautics, Nanjing 211106, China<sup>4</sup>Rocket Force Academy, Beijing 100000, China

Corresponding author: Hai-Lin Chen (hylinchen@126.com)


This work was supported in part by the Start-Up Fund for New Talented Researchers of the Nanjing Vocational University of Industry Technology under Grant YK21-02-01, and in part by the National Science Foundations of China under Grant 61701221.

**ABSTRACT** An improved Alternating-Direction-Implicit iterative algorithm with Gauss-Seidel ideology for efficient weighted-Laguerre-polynomial finite-difference time-domain method is proposed in 3-D cylindrical coordinate system. By transferring the coefficient matrix of the conventional WLP-FDTD equation to the right-side of its equal sign, a linear equation system with ADI characteristic is formed, which makes it more flexible. And then, a correction equation is added to the ADI linear equations and the two-steps Gauss-Seidel procedures are applied to instead of the one-step one in the existing scheme, the purpose of these operations is to speed up the convergence and improve the computation in the term of efficiency and accuracy. Meanwhile, a detailed special treatment scheme for on  $z$ -axis and  $\varphi$ -direction in 3-D cylindrical coordinate system is introduced and discussed, which demonstrates the importance of on  $z$ -axis and  $\varphi$ -direction treatment in the proposed method. In addition, the choice scheme in the term of the time-scaling factor  $s$  and the order of the weighted Laguerre polynomials  $q$  is discussed. Finally, we develop the Perfectly-Matched-Layer implementation to verify the advantage of the proposed method in accuracy. To validate the term of accuracy and efficiency of the proposed method, six numerical examples are provided. At the same time, the discussions of the convergence speed and stability of the proposed method are presented.

**INDEX TERMS** Finite-difference time-domain (FDTD) method, weighted Laguerre polynomial (WLP), altering-direction implicit (ADI), Gauss-Seidel ideology, correction equation.

## I. INTRODUCTION

The basic idea of FDTD (finite-difference time-domain) method is to replace the first-order partial differential of field quantity with the central difference in time and space [1], and to simulate the propagation process of the wave recursively in time-domain, to obtain the field distribution [2], [3]. In other words, the wave equation in time-domain can be directly discredited without any form of derived equation, so its application scope will not be limited by the mathematical model [4], [5]. Based on the above advantages, FDTD

The associate editor coordinating the review of this manuscript and approving it for publication was Ladislav Matekovits .

is widely used in the study of electromagnetic scattering problems [6], [7], [8], and it is very convenient to study electromagnetic problems with arbitrary structures.

Over the years, scholars have used FDTD to study a lot of electromagnetic modeling analyses and calculations for numerous of cylindrical structures in practical applications [9], [10], [11], [12], such as coaxial line, circular waveguide, antenna, missile, aircraft and so on, consisting two broad classes: the symmetrical [13] and the asymmetric structures [14].

(1) Rotating symmetrical structure, also known as the BOR (Body of Revolution), which utilizes the characteristics of axisymmetric, makes the field distribution problem from

three-dimensional (3-D) to two-dimensional (2-D) space. And then, a pure axisymmetric cylindrical structure is formed by the accumulation of different modules [15], [16]. As stated above, it is clear that BOR-FDTD can greatly save computing time and memory consumption. At present, BOR-FDTD is mainly limited to analyzing the closed cavity of the body of revolution in the case of electrically small size and plane wave incidence at small angle [17], moreover, its stability condition is much stricter than that of the 3-D conventional cylindrical coordinate FDTD, which is not only related to the sizes of the time and space steps, but also related to the expansion modulus of the fields [18]. However, in practical engineering applications, the BOR structures are much more complex, and are usually electrically large size, complex and subtle in structure, and coated with medium. There are still many technical problems to be solved before BOR-FDTD can realize such a complex electromagnetic field problem [19], [20]. In order to resolve the above problems, numerous of BOR-FDTD methods are proposed, for example, ADI (alternating-direction implicit)-BOR-FDTD [21], [22], LOD (locally one-dimensional)-BOR-FDTD [23], [24], [25], WCS (weakly conditional stability)-BOR-FDTD [26], [27], HIE (hybrid implicit-explicit)-BOR-FDTD [28], [29] and WLP (weighted Laguerre polynomial)-BOR-FDTD [30], [31], [32] and so on. They can well remove the CFL (courant-friedrichs-lewy) stability condition of the BOR-FDTD method and make the simulation toward BOR structure more efficient, however, the ADI, LOD, WCS and HIE schemes will lead a large numerical dispersion error when the time step is large, and the WLP one will lead to a large amount of memory.

(2) 3-D cylindrical coordinate structure, which can perform central difference operations along the  $\rho$ -,  $\phi$ - and  $z$ -directions. It is also limited by CFL stability condition [33], and it is obvious that the optimization of FDTD method under this kind of structure is difficult. In fact, due to the existence of  $1/\rho$  term in 3-D cylindrical coordinate system, the decomposition of the field along  $\phi$ -direction will lead a large splitting error [34]. How to reduce this kind of error in the iterative FDTD calculation has become a difficult problem. In addition, in the special treatment scheme on the  $z$ -axis and  $\phi$ -direction, how to conduct  $\phi$ -direction transformation of the field on  $z$ -axis and  $\phi$ -direction is also a difficult research in 3-D cylindrical coordinate system [35], [36]. According to the discussion in (1), predecessors have made outstanding contributions to improve the existing BOR-FDTD methods for the problems of 3-D structure and solved numerous of electromagnetic problems. Nevertheless, it should not be ignored that not all cylindrical coordinate structures have rotational symmetry in practical engineering applications. The improved methods of BOR-FDTD in (1) cannot be fully applied to the 3-D cylindrical coordinate asymmetric structures. In a word, it can be said that it is very difficult to study FDTD in 3-D cylindrical coordinate system, perhaps this is why, since 2000, the FDTD methods in 3-D cylindrical coordinate system have not been studied as many as the BOR-FDTD methods.

To solve the problems in (2), An ADI scheme is proposed in 3-D cylindrical coordinate system [37], among, the combination of implicit and explicit differences well solves the stability condition limitation of CFL, which makes the FDTD method become unconditional stability in 3-D cylindrical coordinate system. On this basis, in order to further improve the computational efficiency of the ADI method, a one-step ADI [38] scheme is proposed, which has a greater improvement in efficiency compared with the original ADI [37]. However, the new scheme still cannot avoid the occurrence of numerical dispersion error increasing with time step. Based on the problems in references [37] and [38], we apply a WLP-FDTD scheme (2-D) [39] to the 3-D cylindrical coordinate system, its advantage lies in that it cannot only solve the CFL stability condition limitation, but also reduce the numerical dispersion error. However, its large memory consumption is still a problem to be solved.

In order to further solve many problems of the existing FDTD methods in 3-D cylindrical coordinate system, this paper proposes an improved scheme, which makes the WLP-FDTD method more compact and convergence faster by using the linear iteration characteristics of ADI and the Gauss-Seidel ideology. Meanwhile, the LU decomposition method is further used programmatically to reduce the memory consumption of the proposed method.

The remaining of this paper is organized as follows. In Section II, the equations for the initial values and the iterative procedures of the proposed method are introduced, and some discussions are made about the ADI linear equations. In Section III, the special treatment scheme for fields on the  $z$ -axis and  $\phi$ -direction are introduced, and some analyses and discussions are made about how to determine the final fields for special treatment on  $z$ -axis in the equations of the proposed method. Among Section IV, The advantages in the term of convergence speed and stability of the proposed method are proved. In Section V, some analyses and discussions are given about the choice schemes of  $s$  and  $q$  parameters. In Section VI, the Perfectly-Matched-Layer (PML) implementation for the proposed method is given to validate the advantage of the proposed method in accuracy. Throughout Section VII, numerical examples are given to validate the proposed method. Finally, conclusions are made in Section VIII.

## II. EQUATIONS FOR THE INITIAL VALUES AND THE ITERATIVE PROCEDURES AND SOME DISCUSSIONS

A general arrangement of electromagnetic field components in a 3-D cylindrical coordinate system on the Yee cell is illustrated in Figure 1. In the discrete FDTD computational domain, the cell size in radial, azimuthal, and axial directions are given by  $\Delta\rho$ ,  $\Delta\phi$  and  $\Delta z$ , respectively.

As discussed in [40], the matrix equation of the conventional WLP-FDTD in 3-D cylindrical coordinate system can be written in the following form.

$$(\mathbf{I} - \mathbf{A} - \mathbf{B})\mathbf{W}^q = \mathbf{V}^{q-1} + \mathbf{R}_{JM}^q \quad (1)$$

The derivation of Eq. (1) is shown in Appendix A.

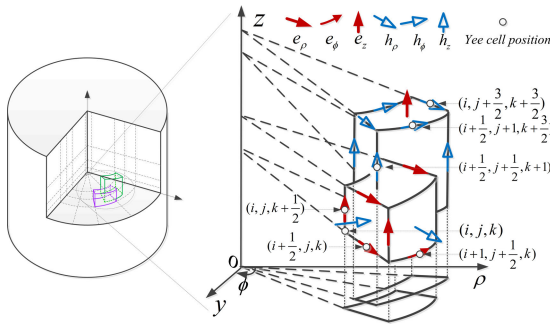


FIGURE 1. Arrangement of electromagnetic field components in cylindrical Yee cell.

Note that

$$\begin{aligned}
 A &= \begin{bmatrix} 0 & A_{\mu\chi} \\ A_{\varepsilon\chi} & 0 \end{bmatrix}, \quad B = \begin{bmatrix} 0 & B_{\mu\chi} \\ B_{\varepsilon\chi} & 0 \end{bmatrix}, \\
 W^q &= [W_E^q \ W_H^q]^T, \quad V^{q-1} = [V_E^{q-1} \ V_H^{q-1}]^T, \\
 W_E^q &= [e_\rho^q \ e_\phi^q \ e_z^q]^T, \\
 V_E^{q-1} &= \left[ -2 \sum e_\rho^\vartheta \ -2 \sum e_\phi^\vartheta \ -2 \sum e_z^\vartheta \right]^T, \\
 W_H^q &= [h_\rho^q \ h_\phi^q \ h_z^q]^T, \\
 V_H^{q-1} &= \left[ -2 \sum h_\rho^\vartheta \ -2 \sum h_\phi^\vartheta \ -2 \sum h_z^\vartheta \right]^T, \\
 A_{\mu\chi} &= \begin{bmatrix} 0 & -a\partial z & 0 \\ 0 & 0 & -a\partial\rho \\ -a(\frac{1}{\rho}\partial\phi) & 0 & 0 \end{bmatrix}, \\
 A_{\varepsilon\chi} &= \begin{bmatrix} 0 & 0 & -b(\frac{1}{\rho}\partial\phi) \\ -b\partial z & 0 & 0 \\ 0 & -b(\frac{1}{\rho}\partial\rho\rho) & 0 \end{bmatrix}, \\
 B_{\mu\chi} &= \begin{bmatrix} 0 & 0 & a(\frac{1}{\rho}\partial\phi) \\ a\partial z & 0 & 0 \\ 0 & a(\frac{1}{\rho}\partial\rho\rho) & 0 \end{bmatrix}, \\
 B_{\varepsilon\chi} &= \begin{bmatrix} 0 & b\partial z & 0 \\ 0 & 0 & b\partial\rho \\ b(\frac{1}{\rho}\partial\phi) & 0 & 0 \end{bmatrix}, \\
 R_{JM}^q &= [R_J^q \ R_M^q]^T = \begin{bmatrix} -aJ_{e\rho}^q & -aJ_{e\phi}^q & -aJ_{e_z}^q \\ bM_{h\rho}^q & bM_{h\phi}^q & bM_{h_z}^q \end{bmatrix}, \\
 a &= \frac{2}{s\varepsilon}, \quad b = \frac{2}{s\mu},
 \end{aligned}$$

where  $s > 0$  is a positive time-scaling factor,  $q$  is the order of the weighted Laguerre polynomials,  $\varepsilon$  and  $\mu$  are the space permittivity and permeability, respectively.  $\partial_i$  is the first-order central difference operator along  $\rho$ -,  $\phi$ - and  $z$ - axes, respectively.  $\sum_{\vartheta=0}^{q-1} \bullet$  represents the sum of the electromagnetic

fields of order 0 to  $q - 1$ , and  $R_{JM}^q$  is the excitation source. Equations for the initial values and the iterative procedures of the proposed method are given in separate situations as follows.

### A. EQUATIONS FOR THE INITIAL VALUES

As discussed in [41], a huge sparse matrix is involved in 3-D conventional cylindrical coordinate WLP-FDTD method. In order to solve it efficiently, a new perturbation  $AB(W^q + W^{q-1})$  is introduced into Eq. (1) [42]. This kind of perturbation show faster convergence, especially at the high-frequency range. Therefore, we can rewrite Eq. (1) as

$$(I - A)(I - B)W^q = -ABW^{q-1} + V^{q-1} + R_{JM}^q. \quad (2)$$

In order to form the two sub-calculation parts of ADI scheme [21], [37] of the proposed method, we introduce the non-physical intermediate variable [43]  $W^{*q} = [W_E^{*q} \ W_H^{*q}]^T$  into Eq. (2), and then, the equations after mathematical transformation can be obtained

$$(I - A)W^{*q} = -BW^{q-1} + V^{q-1} + R_{JM}^q \quad (3a)$$

$$(I - B)W^q = AW^{*q} + V^{q-1} + R_{JM}^q \quad (3b)$$

where  $W^{*q} = [W_E^{*q} \ W_H^{*q}]^T = [e_\rho^{*q} \ e_\phi^{*q} \ e_z^{*q} \ h_\rho^{*q} \ h_\phi^{*q} \ h_z^{*q}]^T$ .

Substituting  $W^{*q} = [W_E^{*q} \ W_H^{*q}]^T$ ,  $V^{q-1} = [V_E^{q-1} \ V_H^{q-1}]^T$  and  $R_{JM}^q$  into Eq. (3a) and Eq. (3b), we can obtain the expansion forms of them as

$$W_E^{*q} - A_{\mu\chi}W_H^{*q} = -B_{\mu\chi}W_H^{q-1} + V_E^{q-1} + R_J^q \quad (4a)$$

$$W_H^{*q} - A_{\varepsilon\chi}W_E^{*q} = -B_{\varepsilon\chi}W_E^{q-1} + V_H^{q-1} + R_M^q \quad (4b)$$

$$W_E^q - B_{\mu\chi}W_H^q = A_{\mu\chi}W_H^{*q} + V_E^{q-1} + R_J^q \quad (4c)$$

$$W_H^q - B_{\varepsilon\chi}W_E^q = A_{\varepsilon\chi}W_E^{*q} + V_H^{q-1} + R_M^q. \quad (4d)$$

In order to construct the first and the second ADI computational steps of the initial values, we substitute the  $W_H^{*q}$  of Eq. (4b) and the  $W_H^q$  of Eq. (4d) into Eq. (4a) and Eq. (4c), respectively, one can obtain

$$\begin{aligned}
 (I - A_{\mu\chi}A_{\varepsilon\chi})W_E^{*q} &= -A_{\mu\chi}B_{\varepsilon\chi}W_E^{q-1} + A_{\mu\chi}V_H^{q-1} \\
 &\quad - B_{\mu\chi}W_H^{q-1} + V_E^{q-1} + R_J^q + A_{\mu\chi}R_M^q \quad (5a)
 \end{aligned}$$

$$W_H^{*q} = A_{\varepsilon\chi}W_E^{*q} - B_{\varepsilon\chi}W_E^{q-1} + V_H^{q-1} + R_M^q \quad (5b)$$

$$\begin{aligned}
 (I - B_{\mu\chi}B_{\varepsilon\chi})W_E^q &= B_{\mu\chi}A_{\varepsilon\chi}W_E^{*q} + B_{\mu\chi}V_H^{q-1} \\
 &\quad + A_{\mu\chi}W_H^{*q} + V_E^{q-1} + R_J^q + B_{\mu\chi}R_M^q \quad (6a)
 \end{aligned}$$

$$W_H^q = B_{\varepsilon\chi}W_E^q + A_{\varepsilon\chi}W_E^{*q} + V_H^{q-1} + R_M^q. \quad (6b)$$

Combining with Gauss-Seidel ideology, and expanding Eq. (5a), we can obtain the electric field equations of the

non-physical intermediate variable as

$$\begin{aligned} (\mathbf{I} - ab\partial z^2) e_\rho^{*q} &= ab\partial z\partial\rho e_z^{q-1} + 2a\partial z \sum h_z^q \\ &\quad - a\left(\frac{1}{\rho}\partial\phi\right)h_z^{q-1} - 2\sum e_\rho^q + \mathbf{R}_{in-1}^q \end{aligned} \quad (5a-1)$$

$$\begin{aligned} \left(\mathbf{I} - ab\partial\rho\left(\frac{1}{\rho}\partial\phi\right)\right) e_\phi^{*q} &= ab\partial\rho\left(\frac{1}{\rho}\partial\phi\right)e_\rho^{q-1} + 2a\partial\rho \sum h_z^q \\ &\quad - a\partial zh_\rho^{q-1} - 2\sum e_\phi^q + \mathbf{R}_{in-2}^q \end{aligned} \quad (5a-2)$$

$$\begin{aligned} \left(\mathbf{I} - ab\left(\frac{1}{\rho}\partial\phi\right)^2\right) e_z^{*q} &= ab\left(\frac{1}{\rho}\partial\phi\right)\partial z e_\phi^{q-1} + 2a\left(\frac{1}{\rho}\partial\phi\right) \sum h_\rho^q \\ &\quad - a\left(\frac{1}{\rho}\partial\rho\right)h_\phi^{q-1} - 2\sum e_z^q + \mathbf{R}_{in-3}^q \end{aligned} \quad (5a-3)$$

where

$$\mathbf{R}_{in-1}^q = -aJ_{e\rho}^q - ab\partial z M_{h\phi}^q \quad (5a-1s)$$

$$\mathbf{R}_{in-2}^q = -aJ_{e\phi}^q - ab\partial\rho M_{hz}^q \quad (5a-2s)$$

$$\mathbf{R}_{in-3}^q = -aJ_{e_z}^q - ab\left(\frac{1}{\rho}\partial\phi\right)M_{h\rho}^q \quad (5a-3s)$$

the group of Eq. (5a-1s) to Eq. (5a-3s) consists the excitation sources of the non-physical intermediate variable in the initial values.

The applications of Gauss-Seidel ideology have been shown in the group of Eq. (5a-1) to Eq. (5a-3), namely, we replace  $e_\rho^{q-1}$  in the right-side of Eq. (5a-2) with  $-e_\rho^{*q}$  as solved by Eq. (5a-1), similarly, we use  $-e_\phi^{*q}$  from Eq. (5a-2) to replace  $e_\phi^{q-1}$  of Eq. (5a-3). Obviously, the procedures of Eq. (5a-1) to Eq. (5a-3) will influence the form of Eq. (5b), thus the new matrix form of Eq. (5b) can be shown as

$$\mathbf{W}_H^{*q} = \mathbf{A}_{\varepsilon\chi} \mathbf{W}_E^{*q} - \mathbf{B}_{\varepsilon\chi} \mathbf{W}_{E_{new1}}^{q-1} + \mathbf{V}_H^{q-1} + \mathbf{R}_M^q \quad (5c)$$

where  $\mathbf{W}_{E_{new1}}^{q-1} = \begin{bmatrix} -e_\rho^{*q} & -e_\phi^{*q} & e_z^{q-1} \end{bmatrix}^T$ .

Expanding Eq. (5c), the magnetic field equations of the non-physical intermediate variable can be obtained as

$$h_\rho^{*q} = -b\left(\frac{1}{\rho}\partial\phi\right)e_z^{*q} + b\partial z e_\phi^{*q} - 2\sum h_\rho^\vartheta + bM_{h\rho}^q \quad (5c-1)$$

$$h_\phi^{*q} = -b\partial z e_\rho^{*q} - b\partial\rho e_z^{q-1} - 2\sum h_\phi^\vartheta + bM_{h\phi}^q \quad (5c-2)$$

$$h_z^{*q} = -b\left(\frac{1}{\rho}\partial\rho\right)e_\phi^{*q} + b\left(\frac{1}{\rho}\partial\phi\right)e_\rho^{*q} - 2\sum h_z^\vartheta + bM_{hz}^q. \quad (5c-3)$$

Clearly, the group of Eq. (5a) and Eq. (5c) form a new combination, which actually constructs the first computational step of the initial values in the proposed method.

Similarly, referring to Eq. (5c), we can obtain the new form of Eq. (6b) as

$$\mathbf{W}_H^q = \mathbf{B}_{\varepsilon\chi} \mathbf{W}_E^q + \mathbf{A}_{\varepsilon\chi} \mathbf{W}_{E_{new2}}^{*q} + \mathbf{V}_H^{q-1} + \mathbf{R}_M^q \quad (6c)$$

where  $\mathbf{W}_{E_{new2}}^{*q} = \begin{bmatrix} e_\rho^{*q} & e_\phi^q & e_z^q \end{bmatrix}^T$ .

Obviously, the group of Eq. (6a) and Eq. (6c) form another new combination, which actually constructs the second computational step of the initial values in the proposed method.

Expanding Eq. (6a) and applying the Gauss-Seidel procedures directly, we can obtain

$$\begin{aligned} \left(\mathbf{I} - ab\left(\frac{1}{\rho}\partial\rho\right)(\partial\rho)\right) e_z^q &= -ab\left(\frac{1}{\rho}\partial\rho\right)(\partial z) e_\rho^{*q} \\ &\quad - 2a\left(\frac{1}{\rho}\partial\rho\right) \sum h_\phi^q - a\left(\frac{1}{\rho}\partial\phi\right)h_\rho^{*q} \\ &\quad - 2\sum e_z^q + \mathbf{R}_{in-4}^q \end{aligned} \quad (6a-1)$$

$$\begin{aligned} (\mathbf{I} - ab\partial z^2) e_\phi^q &= -ab\partial z\left(\frac{1}{\rho}\partial\phi\right)e_\rho^{*q} - 2a\partial z \sum h_\rho^q \\ &\quad - a\partial\rho h_z^{*q} - 2\sum e_\phi^q + \mathbf{R}_{in-5}^q \end{aligned} \quad (6a-2)$$

$$\begin{aligned} \left(\mathbf{I} - ab\left(\frac{1}{\rho}\partial\phi\right)^2\right) e_\rho^q &= -ab\left(\frac{1}{\rho}\partial\phi\right)\left(\frac{1}{\rho}\partial\rho\right)e_\phi^{*q} \\ &\quad - 2a\left(\frac{1}{\rho}\partial\phi\right) \sum h_z^q - a\partial z h_\phi^{*q} - 2\sum e_\rho^q + \mathbf{R}_{in-6}^q \end{aligned} \quad (6a-3)$$

where

$$\mathbf{R}_{in-4}^q = -aJ_{e_z}^q + ab\left(\frac{1}{\rho}\partial\rho\right)M_{h\phi}^q \quad (6a-1s)$$

$$\mathbf{R}_{in-5}^q = -aJ_{e_\phi}^q + ab\partial z M_{h\rho}^q \quad (6a-2s)$$

$$\mathbf{R}_{in-6}^q = -aJ_{e_\rho}^q + ab\left(\frac{1}{\rho}\partial\phi\right)M_{hz}^q. \quad (6a-3s)$$

Eq. (6a-1s) - Eq. (6a-3s) are also the excitation sources.

The procedures of Eq. (6a-1) to Eq. (6a-3) are similar with the ones of Eq. (5a-1) to Eq. (5a-3), we replace  $e_z^{*q}$  in the right-side of Eq. (6a-2) with  $e_z^q$ , which has been obtained by Eq. (6a-1). Similarly,  $e_\phi^{*q}$  in the right-side of Eq. (6a-3) is replaced by  $e_\phi^q$ .

Expanding Eq. (6c), we can obtain the magnetic field equations as

$$h_\rho^q = b\partial z e_\phi^q - b\left(\frac{1}{\rho}\partial\phi\right)e_z^q - 2\sum h_\rho^\vartheta + bM_{h\rho}^q \quad (6c-1)$$

$$h_\phi^q = b\partial\rho e_z^q - b\partial z e_\rho^{*q} - 2\sum h_\phi^\vartheta + bM_{h\phi}^q \quad (6c-2)$$

$$h_z^q = b\left(\frac{1}{\rho}\partial\phi\right)e_\rho^q - b\left(\frac{1}{\rho}\partial\rho\right)e_\phi^q - 2\sum h_z^\vartheta + bM_{hz}^q. \quad (6c-3)$$

So far, the first and second computational steps of the initial values have been explained completely, and the Gauss-Seidel ideology has been well applied. However, seeing the

procedures of Eq. (5a-1) to Eq. (5a-3) again, we find that  $e_z^{q-1}$  in the right-side of Eq. (5a-1) is not replaced by Gauss-Seidel ideology. This situation will become a hidden trouble which will affect the convergence speed and calculation in the term of efficiency and accuracy. To avoid it, we add a correction term to connect the first and the second computational steps of the initial values in the proposed method. This correction equation is given as

$$(\mathbf{I} - ab\partial z^2)e_\rho^{*q} = ab\partial z\partial\rho(-e_z^{*q}) + 2a\partial z \sum h_z^\vartheta - a\left(\frac{1}{\rho}\partial\phi\right)h_z^{q-1} - 2 \sum e_\rho^\vartheta + \mathbf{R}_{in-7}^q \quad (7)$$

in which  $\mathbf{R}_{in-7}^q = -a\mathbf{J}_{e\rho}^q - ab\partial z\mathbf{M}_{h\phi}^q$ .

In fact,  $e_z^{*q}$  in the right-side of Eq. (7) is solved by Eq. (5a-3), and then,  $e_z^{q-1}$  in the right-side of Eq. (5a-1) is replaced with  $-e_z^{*q}$ .

Therefore, the computation sequence of the initial values in the proposed method is Eq. (5a-1) to Eq. (5a-3) → Eq. (5c-1) to Eq. (5c-3) → Eq. (7) → Eq. (6a-1) to Eq. (6a-3) → Eq. (6c-1) to Eq. (6c-3). Note that, because we add the correction term Eq. (7), so the computation sequence of Eq. (6a-1) to Eq. (6a-3) cannot be changed.

### B. EQUATIONS FOR THE ITERATIVE PROCEDURES

In retrospect, we have referred to reference [42] and introduced the perturbation term  $\mathbf{AB}(W^q + W^{q-1})$  into the initial values. Clearly, the Gauss-Seidel procedures in Eq. (5a) make the electric field components negative. Therefore, we define  $W_p^q$  as the solved result of the  $p$ -th iteration of Eq. (2) after using the Gauss-Seidel procedure. At the same time, the new perturbation term  $\mathbf{AB}(W_{p+1}^q - W_p^q)$  is introduced to modify the original one.

Substituting  $\mathbf{AB}(W_{p+1}^q - W_p^q)$  into Eq. (1), we can obtain

$$(\mathbf{I} - \mathbf{A})(\mathbf{I} - \mathbf{B})W_{p+1}^q = \mathbf{AB}W_p^q + V^{q-1} + \mathbf{R}_{JM}^q. \quad (8)$$

Eq. (8) can be split into two steps as

$$(\mathbf{I} - \mathbf{A})W_{p+1}^q = \mathbf{B}W_p^q + V^{q-1} + \mathbf{R}_{JM}^q \quad (9a)$$

$$(\mathbf{I} - \mathbf{B})W_{p+1}^q = \mathbf{A}W_{p+1}^q + V^{q-1} + \mathbf{R}_{JM}^q \quad (9b)$$

where  $W_{p+1}^q = \begin{bmatrix} e_{\rho,p+1}^{*q} & e_{\phi,p+1}^{*q} & e_{z,p+1}^{*q} & h_{\rho,p+1}^{*q} & h_{\phi,p+1}^{*q} & h_{z,p+1}^{*q} \end{bmatrix}^T$  is the non-physical intermediate variable, and the subscript  $p$  is the  $p$ -th iteration.

Defining  $W_p^q = \begin{bmatrix} W_{E,p}^q & W_{H,p}^q \end{bmatrix}^T$  and  $W_p^{*q} = \begin{bmatrix} W_{E,p}^{*q} & W_{H,p}^{*q} \end{bmatrix}^T$ , Eq. (9a) and Eq. (9b) can be expanded as

$$W_{E,p+1}^q - A_{\mu\chi} W_{H,p+1}^q = B_{\mu\chi} W_{H,p}^q + V_E^{q-1} + R_J^q \quad (10a)$$

$$W_{H,p+1}^q - A_{\varepsilon\chi} W_{E,p+1}^q = B_{\varepsilon\chi} W_{E,p}^q + V_H^{q-1} + R_M^q \quad (10b)$$

$$W_{E,p+1}^q - B_{\mu\chi} W_{H,p+1}^q = A_{\mu\chi} W_{H,p+1}^q + V_E^{q-1} + R_J^q \quad (10c)$$

$$W_{H,p+1}^q - B_{\varepsilon\chi} W_{E,p+1}^q = A_{\varepsilon\chi} W_{E,p+1}^q + V_H^{q-1} + R_M^q. \quad (10d)$$

Substituting  $W_{H,p+1}^{*q}$  of Eq. (10b) into Eq. (10a), we can obtain the first computational step of the iterative procedures as

$$\begin{aligned} & (\mathbf{I} - A_{\mu\chi}A_{\varepsilon\chi})W_{E,p+1}^{*q} \\ & = A_{\mu\chi}B_{\varepsilon\chi}W_{E,p}^q + B_{\mu\chi}W_{H,p}^q + A_{\mu\chi}V_H^{q-1} \\ & \quad + V_E^{q-1} + A_{\mu\chi}R_M^q + R_J^q \end{aligned} \quad (11a)$$

$$W_{H,p+1}^{*q} = B_{\varepsilon\chi}W_{E,p}^q + A_{\varepsilon\chi}W_{E,p+1}^{*q} + V_H^{q-1} + R_M^q. \quad (11b)$$

Note that, because the applying of the Gauss-Seidel ideology in Eq. (11a), so Eq. (11b) should be modified, the modification way is similar to Eq. (5c). For simplicity, it is not listed here, we can obtain directly

$$W_{H,p+1}^{*q} = B_{\varepsilon\chi}W_{E_{new1,p}}^q + A_{\varepsilon\chi}W_{E,p+1}^{*q} + V_H^{q-1} + R_M^q \quad (11c)$$

where  $W_{E_{new1,p}}^q = \begin{bmatrix} e_{\rho,p+1}^{*q} & e_{\phi,p+1}^{*q} & e_{z,p}^q \end{bmatrix}^T$ .

According to the detailed derivation of Eq. (5a-1) to Eq. (5a-3) in Part A of this section, we can directly expand Eq. (11a) and apply the Gauss-Seidel procedures

$$\begin{aligned} & (\mathbf{I} - ab\partial z^2)e_{\rho,p+1}^{*q} \\ & = -ab\partial z\partial\rho e_{z,p}^q + a\left(\frac{1}{\rho}\partial\phi\right)h_{z,p}^q + 2a\partial z \sum h_\phi^\vartheta - 2 \sum e_\rho^\vartheta \\ & \quad - ab\partial zM_{h\phi}^q - aJ_{e\rho}^q \end{aligned} \quad (11a-1)$$

$$\begin{aligned} & \left(\mathbf{I} - ab\partial\rho\left(\frac{1}{\rho}(\partial\rho)\rho\right)\right)e_{\phi,p+1}^{*q} \\ & = -ab\partial\rho\left(\frac{1}{\rho}\partial\phi\right)e_{\rho,p+1}^{*q} + a\partial z h_{\rho,p}^q + 2a\partial z \sum h_\phi^\vartheta - 2 \sum e_\rho^\vartheta \\ & \quad - ab\partial\rho M_{hz}^q - aJ_{e\phi}^q \end{aligned} \quad (11a-2)$$

$$\begin{aligned} & \left(\mathbf{I} - ab\left(\frac{1}{\rho}\partial\phi\right)^2\right)e_{z,p+1}^{*q} \\ & = -ab\left(\frac{1}{\rho}(\partial\rho)\partial z e_{\phi,p+1}^{*q} + a\left(\frac{1}{\rho}(\partial\rho)\rho\right)h_{\phi,p}^q\right) \\ & \quad + 2a\left(\frac{1}{\rho}\partial\phi\right) \sum h_\rho^\vartheta - 2 \sum e_z^\vartheta - ab\left(\frac{1}{\rho}\partial\phi\right)M_{h\rho}^q - aJ_{e_z}^q. \end{aligned} \quad (11a-3)$$

Expanding Eq. (11c), we can obtain

$$h_{\rho,p+1}^{*q} = b\partial z e_{\phi,p+1}^{*q} - b\left(\frac{1}{\rho}\partial\phi\right)e_{z,p+1}^{*q} - 2 \sum h_\rho^\vartheta + bM_{h\rho}^q \quad (11c-1)$$

$$h_{\phi,p+1}^{*q} = b\partial\rho e_{z,p}^q - b\partial z e_{\rho,p+1}^{*q} - 2 \sum h_\phi^\vartheta + bM_{h\phi}^q \quad (11c-2)$$

$$h_{z,p+1}^{*q} = b\left(\frac{1}{\rho}\partial\phi\right)e_{\rho,p+1}^{*q} - b\left(\frac{1}{\rho}(\partial\rho)\rho\right)e_{\phi,p+1}^{*q} - 2 \sum h_z^\vartheta + bM_{hz}^q. \quad (11c-3)$$

At this point, we have explained the first computational step of the iterative procedures completely.



Similarly, we also need to add a correction term

$$\begin{aligned} & (\mathbf{I} - ab\partial z^2)e_{\rho,p+1}^{*q} \\ &= -ab\partial z\partial\rho e_{z,p+1}^{*q} + a\left(\frac{1}{\rho}\partial\phi\right)h_{z,p}^q + 2a\partial z\sum h_{\phi}^{\vartheta} - 2\sum e_{\rho}^{\vartheta} \\ & \quad - ab\partial zM_{h\phi}^q - aJ_{e\rho}^q \end{aligned} \quad (12)$$

where  $e_{z,p+1}^{*q}$  of the right-side in Eq. (12) is solved by Eq. (11a-3), and the solution of Eq. (12) will be used to connect the second computational step of the iterative procedures of the proposed method.

Then, we substitute  $\mathbf{W}_{H,p+1}^q$  of Eq. (10d) into Eq. (10c). We can update the second computational step of the iterative procedures as

$$\begin{aligned} & (\mathbf{I} - \mathbf{B}_{\mu\chi}\mathbf{B}_{\varepsilon\chi})\mathbf{W}_{E,p+1}^q \\ &= \mathbf{B}_{\mu\chi}\mathbf{A}_{\varepsilon\chi}\mathbf{W}_{E,p+1}^{*q} + \mathbf{A}_{\mu\chi}\mathbf{W}_{H,p+1}^{*q} + \mathbf{B}_{\mu\chi}\mathbf{V}_H^{q-1} \\ & \quad + \mathbf{V}_E^{q-1} + \mathbf{B}_{\mu\chi}\mathbf{R}_M^q + \mathbf{R}_J \end{aligned} \quad (13a)$$

$$\mathbf{W}_{H,p+1}^q = \mathbf{A}_{\varepsilon\chi}\mathbf{W}_{Enew2,p+1}^{*q} + \mathbf{B}_{\varepsilon\chi}\mathbf{W}_{E,p+1}^q + \mathbf{V}_H^{q-1} + \mathbf{R}_M^q. \quad (13b)$$

For the sake of simplicity, we directly update Eq. (10d) to Eq. (13b), the process will not be repeated here (please refer to the processes of Eq. (5c), Eq. (6c) and Eq. (11c)). That is to say, due to the applications of the Gauss-Seidel in Eq. (13a), we replace  $\mathbf{W}_{E,p+1}^{*q} = \begin{bmatrix} e_{\rho,p+1}^{*q} & e_{\phi,p+1}^{*q} & e_{z,p+1}^{*q} \end{bmatrix}^T$  of Eq. (10d) with  $\mathbf{W}_{Enew2,p+1}^{*q} = \begin{bmatrix} e_{\rho,p+1}^{*q} & e_{\phi,p+1}^q & e_{z,p+1}^q \end{bmatrix}^T$  of Eq. (13b).

Expanding Eq. (13a) and Eq. (13b), we can obtain

$$\begin{aligned} & \left(\mathbf{I} - ab\left(\frac{1}{\rho}(\partial\rho)\rho\right)\partial\rho\right)e_{z,p+1}^q \\ &= -ab\left(\frac{1}{\rho}(\partial\rho)\rho\right)\partial z e_{\rho,p+1}^{*q} - a\left(\frac{1}{\rho}(\partial\phi)\right)h_{\rho,p+1}^{*q} - 2\sum e_z^{\vartheta} \\ & \quad - 2a\left(\frac{1}{\rho}(\partial\rho)\rho\right)\sum h_{\phi}^{\vartheta} + ab\left(\frac{1}{\rho}(\partial\rho)\rho\right)M_{h\phi}^q - aJ_{ez}^q \end{aligned} \quad (13a-1)$$

$$\begin{aligned} & \left(\mathbf{I} - ab\partial z^2\right)e_{\phi,p+1}^q \\ &= -ab\partial z\left(\frac{1}{\rho}\partial\phi\right)e_{z,p+1}^q - a\partial\rho h_{z,p+1}^{*q} - 2a\partial z\sum h_{\rho}^{\vartheta} \\ & \quad - 2\sum e_{\phi}^{\vartheta} + ab\partial zM_{h\rho}^q - aJ_{e\phi}^q \end{aligned} \quad (13a-2)$$

$$\begin{aligned} & \left(\mathbf{I} - ab\left(\frac{1}{\rho}(\partial\phi)^2\right)\right)e_{\rho,p+1}^q \\ &= -ab\left(\frac{1}{\rho}(\partial\phi)\right)\left(\frac{1}{\rho}(\partial\rho)\rho\right)e_{\phi,p+1}^q - a\partial z h_{\phi,p+1}^{*q} \\ & \quad - 2a\left(\frac{1}{\rho}(\partial\phi)\right)\sum h_z^{\vartheta} - 2\sum e_{\rho}^{\vartheta} - ab\left(\frac{1}{\rho}(\partial\phi)\right)M_{hz}^q - aJ_{e\rho}^q \end{aligned} \quad (13a-3)$$

$$\begin{aligned} & h_{\rho,p+1}^q \\ &= -b\left(\frac{1}{\rho}\partial\phi\right)e_{z,p+1}^q - b\partial z e_{\phi,p+1}^q - 2\sum h_{\rho}^{\vartheta} + bM_{h\rho}^q \end{aligned} \quad (13b-1)$$

$$\begin{aligned} & h_{\phi,p+1}^q \\ &= -b\partial z e_{\rho,p+1}^{*q} + b\partial\rho e_{z,p+1}^q - 2\sum h_{\phi}^{\vartheta} + bM_{h\phi}^q \end{aligned} \quad (13b-2)$$

$$\begin{aligned} & h_{z,p+1}^q \\ &= -b\left(\frac{1}{\rho}(\partial\rho)\rho\right)e_{\phi,p+1}^q + b\left(\frac{1}{\rho}\partial\phi\right)e_{\rho,p+1}^q - 2\sum h_z^{\vartheta} + bM_{hz}^q. \end{aligned} \quad (13b-3)$$

So far, the iterative procedures of the proposed method have been explained completely. For easier understanding, the overall execution process of the iterative procedures is presented here, as shown in Figure 2.

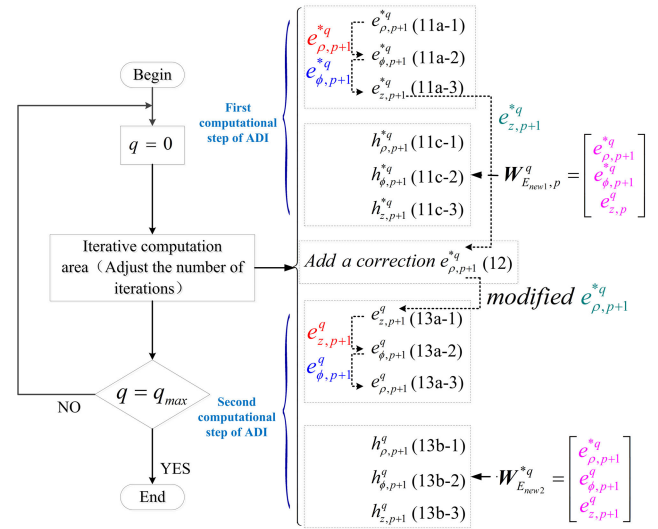


FIGURE 2. Overall execution process of the iterative procedures.

The computation sequence of the iterative procedures in the proposed method is Eq. (11a-1) to Eq. (11a-3) → Eq. (11c-1) to Eq. (11c-3) → Eq. (12) → Eq. (13a-1) to Eq. (13a-3) → Eq. (13b-1) to Eq. (13b-3). Similarly, the computation sequence of Eq. (13a-1) to Eq. (13a-3) cannot be changed.

The ways of the first-order central difference expansions are explained in Appendix B.

### C. DISCUSSION FOR THE ADI LINEAR EQUATIONS

Eq. (1) is the matrix form of the conventional WLP-FDTD in 3-D cylindrical coordinate system. Here, we convert it into a general form as follow

$$[\xi][\delta] = [\psi] \quad (14)$$

where  $[\xi]$  is the coefficient matrix associated with the central difference operation  $(\mathbf{I} - \mathbf{A} - \mathbf{B})$ ,  $[\delta]$  is a column vector constituted by unknown electric- and magnetic- field values, and  $[\psi]$  is a known column vector constituted by the sum of the electric- and magnetic- fields of order 0 to  $q-1$  on the right-side of Eq. (1).

In the following, we take the matrix equations of two computational steps in the iterative procedures as examples for discussions.

Seeing Eq. (9a) again, we find that all the vectors of the right-side in Eq. (9a) are known, thus, Eq. (9a) is actually the iterative solution of a linear equation system. Analogously, because  $\mathbf{W}_{p+1}^{*q}$  has been solved by Eq. (9a), so all the vectors of the right-side in Eq. (9b) are known, further, we can say that Eq. (9b) is also the iterative solution of a linear equation system.

Obviously, the non-physical intermediate variable changes Eq. (1) from the general form of a linear equation system (see Eq. (14)) to a new one with the characteristics of ADI. Indeed, the matrix forms of Eq. (9a) and Eq. (9b) can be understood as Eq. (9a) moves the  $\mathbf{B}$  operator to the right-side of Eq. (14), while Eq. (9b) moves the  $\mathbf{A}$  operator to the right-side of Eq. (14).

In other words, the two computational steps of the proposed method are actually the ADI iterative linear equations, and they are more flexible.

### III. SPECIAL TREATMENT SCHEME ON THE Z-AXIS AND THE FDTD DIFFERENCE IN THE $\phi$ -DIRECTION

According to the characteristics of the Yee cell, the unknown electric- or magnetic- field on the grid point of integer of the unit's Yee cell can be solved by the known electric- or magnetic- field on its surrounding half grid point. In cylindrical architecture shown in Figure 3, when  $\rho = 0$ , all the electric- and the magnetic- fields along the  $z$ -axis are mathematically singularity [35], they should be treated specially, otherwise, there will be a large splitting error in FDTD methods [36].

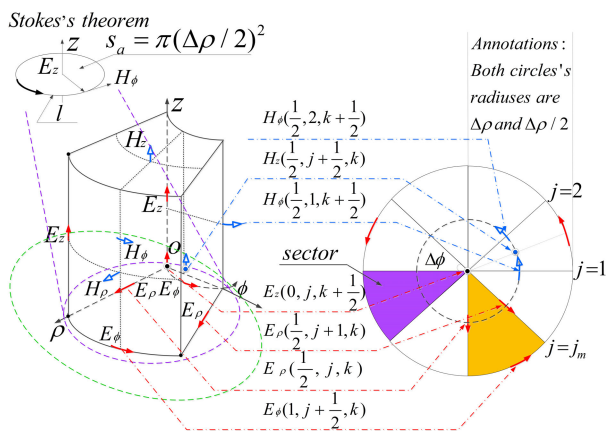


FIGURE 3. Top view of the field components nearby the z-axis.

In addition, the circle of Figure 3 shows that the fields in the 3-D cylindrical coordinate system are regarded as periodic in the  $\phi$ -direction. Therefore, it is necessary to connect the fields at a specific plane in the  $\phi$ -direction using the periodic boundary condition when the FDTD central difference operation is performed on a field in the  $\phi$ -direction. We also should treat them specially, otherwise, there will be a large splitting error too [44].

### A. PRINCIPLE ANALYSIS OF THE SPECIAL TREATMENT SCHEME FOR ON-AXIS FIELDS

In fact, the special treatment scheme on the  $z$ -axis of a 3-D cylindrical coordinate asymmetric structure is different with the BOR one. For example, in the BOR structure, because 3-D Yee cells have been converted into 2-D problems for processing, the fields near the  $z$ -axis do not need to consider the change of  $\phi$ -direction [15], [16]. However, as shown in Figure 3, in the 3-D cylindrical coordinate asymmetric structure, when we analyze the electrical- and the magnetic- fields near the  $z$ -axis, the change of  $\phi$ -direction must be considered.

In Figure 3, it can be clearly seen that the section  $\rho\phi$  of the field units is a partial circular ring. And the section of the field units adjacent to the  $z$ -axis can be degenerated from a partial circular ring to a sector (such as the purple sector). Furthermore, as shown in the right-part of Figure 3, the difference grids on the  $z$ -axis can be obtained by adding up the sectors corresponding to different  $j$ . Therefore, all the electric- and the magnetic- difference equations on the  $z$ -axis require special treatment [35], [36]. However, for all the electric- and the magnetic- fields near the  $z$ -axis, since the directions of  $E_\rho, E_\phi, H_\rho$  and  $H_\phi$  vary with  $\phi$ , they are meaningless on the  $z$ -axis. So, there are only  $E_z(0, j, k + \frac{1}{2})$  and  $H_z(\frac{1}{2}, j + \frac{1}{2}, k)$  in the proposed method need special treatment on the  $z$ -axis.

### B. TREATMENT EQUATIONS OF THE SPECIAL TREATMENT SCHEME FOR ON-AXIS FIELDS

As shown in Figure 3, and according to the Stokes' theorem, the integral equation of electric-field in the frequency-domain can be obtained

$$j\omega\epsilon \int_{s_a} \vec{E}_z ds = \oint_l \vec{H} \cdot d\vec{l}. \quad (15)$$

Denoting  $s_a$  is the area integral region and  $l$  is the line integral path along the  $s_a$  plane.

In the same way, the integral equation of magnetic-field in the frequency-domain can be obtained as

$$j\omega\mu \int_{s_a} \vec{H}_z ds = - \oint_l \vec{E} \cdot d\vec{l}. \quad (16)$$

Seeing again to the right-part of Figure 3, if radiuses of the integral region of the circles are  $\frac{\Delta\rho}{2}$  and  $\Delta\rho$  respectively, then Eq. (15) and Eq. (16) can be transformed into the difference equations.

$$\epsilon\pi \frac{\Delta\rho^2}{4} \frac{\partial E_z(0, j, k + \frac{1}{2})}{\partial t} = \frac{\Delta\rho\Delta\phi}{2} \sum_{j_c=1}^{j_m} H_\phi(\frac{1}{2}, j_c, k + \frac{1}{2}) \quad (15a)$$

$$\frac{\mu\pi\Delta\rho\Delta\phi}{2\pi} \frac{\partial H_z(\frac{1}{2}, j + \frac{1}{2}, k)}{\partial t} = \left[ E_\rho(\frac{1}{2}, j+1, k) - E_\rho(\frac{1}{2}, j, k) \right] - \Delta\phi \sum_{j_c=1}^{j_m} E_\phi(1, j_c + \frac{1}{2}, k) \quad (16a)$$

It is worth noting that the form of Eq. (16a) is slightly different from Eq. (15a). The reason is that, as shown in the orange sector on the right-part of Figure 3, the transmission directions of  $E_\rho$  and  $E_\phi$  form a closed sector. In the process of adding different sectors,  $E_\rho$  cancels out each other. Therefore, Eq. (16a) only left  $E_\phi$ , and  $E_\phi$  has no actual physical significance near the  $z$ -axis, that is to say,  $H_z$  actually does not need special treatment.

By introducing the WLP technology [40] into Eq. (15a), we can obtain

$$\begin{bmatrix} E_z^q(0, j, k + \frac{1}{2}) \\ +2 \sum E_z^\vartheta(0, j, k + \frac{1}{2}) \end{bmatrix} = \frac{2a\Delta\phi}{\pi\Delta\rho} \sum_{j_c=1}^{j_m} H_\phi^q(\frac{1}{2}, j_c, k + \frac{1}{2}) \quad (15b)$$

where  $E_z^q$  is  $e_z^{*q}$  or  $e_z^q$ , and  $H_\phi^q$  is  $h_\phi^{*q}$  or  $H_\phi^{*q}$ , which are depended on whether the non-physical intermediate variables need to be calculated on the  $z$ -axis.

For example as Eq. (13b-2) in the Part B of Section II, when  $\rho = 0$ , we can obtain  $h_{\phi, p+1}^q(\frac{1}{2}, j, k + \frac{1}{2})$  as

$$\begin{aligned} & h_{\phi, p+1}^q(\frac{1}{2}, j, k + \frac{1}{2}) \\ &= \frac{b}{\Delta\rho} \begin{bmatrix} e_{z, p+1}^q(1, j, k + \frac{1}{2}) \\ -e_{z, p+1}^q(0, j, k + \frac{1}{2}) \end{bmatrix} - \frac{b}{\Delta z} \begin{bmatrix} e_{\rho, p+1}^{*q}(\frac{1}{2}, j, k + 1) \\ -e_{\rho, p+1}^{*q}(\frac{1}{2}, j, k) \end{bmatrix} \\ & - 2 \sum h_\phi^\vartheta(\frac{1}{2}, j, k + \frac{1}{2}) + bM_{h\phi}^q(\frac{1}{2}, j, k + \frac{1}{2}). \quad (17) \end{aligned}$$

Substituting Eq. (17) into Eq. (15b), we can obtain the final equation of the special treatment for on  $z$ -axis in the iterative procedures of the proposed method.

$$\begin{aligned} & \begin{pmatrix} (1 + \frac{2j_m ab \Delta\phi}{\pi \Delta\rho^2}) e_{z, p+1}^q(0, j_c, k + \frac{1}{2}) \\ -\frac{2ab\Delta\phi}{\pi \Delta\rho^2} \sum_{j_c=1}^{j_m} e_{z, p+1}^q(1, j_c, k + \frac{1}{2}) \end{pmatrix} \\ &= -\frac{2ab\Delta\phi}{\pi \Delta\rho \Delta z} \sum_{j_c=1}^{j_m} \left[ e_{\rho, p+1}^{*q}(\frac{1}{2}, j_c, k + 1) - e_{\rho, p+1}^{*q}(\frac{1}{2}, j_c, k) \right] \\ & - \frac{4a\Delta\phi}{\pi \Delta\rho} \sum_{j_c=1}^{j_m} \left[ \sum h_\phi^k(\frac{1}{2}, j_c, k + \frac{1}{2}) \right] \\ & - 2 \sum e_z^\vartheta(\frac{1}{2}, j_c, k + \frac{1}{2}) \\ & + \frac{2ab\Delta\phi}{\pi \Delta\rho} \sum_{j_c=1}^{j_m} M_{h\phi}^q(\frac{1}{2}, j_c, k + \frac{1}{2}) \quad (18) \end{aligned}$$

where  $(1 + \frac{2j_m ab \Delta\phi}{\pi \Delta\rho^2}) e_{z, p+1}^q(0, j_c, k + \frac{1}{2})$  in the left-side of Eq. (18) is the result of the combination of  $e_{z, p+1}^q(0, j, k + \frac{1}{2})$

and  $\sum_{j_c=1}^{j_m} e_{z, p+1}^q(0, j_c, k + \frac{1}{2})$ .

Unfortunately, since  $e_{z, p+1}^q$  in the left-side of Eq. (18) has  $(j_m + 1)$  terms, it cannot form a tridiagonal equation for easy

solution, so, we need an approximate iterative method here. Therefore, the left-side of Eq. (18) can be rewritten as

$$\begin{aligned} & \begin{pmatrix} (1 + \frac{2j_m ab \Delta\phi}{\pi \Delta\rho^2}) e_{z, p+1}^q(0, j, k + \frac{1}{2}) \\ -\frac{2ab\Delta\phi}{\pi \Delta\rho^2} e_{z, p+1}^q(1, j, k + \frac{1}{2}) \end{pmatrix} \\ &= \frac{2ab\Delta\phi}{\pi \Delta\rho^2} \sum_{j_d=1}^{j_m} e_{z, p+1}^q(1, j_d, k + \frac{1}{2}) + L(i_L = 0 \text{ or } \frac{1}{2}, j, k). \quad (19) \end{aligned}$$

Here,  $L(i_L = 0 \text{ or } \frac{1}{2}, j, k)$  is the last term in the right-side of Eq. (19), which includes all the terms in the right-side of Eq. (18).  $\frac{2ab\Delta\phi}{\pi \Delta\rho^2} \sum_{j_d=1}^{j_m} e_{z, p+1}^q(1, j_d, k + \frac{1}{2})$  is the result of moving the left-side of Eq. (18) to the right-side of Eq. (19), where  $j$  is not included in  $j_d$ . Undeniably, this is an approximate iterative method for constructing a tridiagonal equation, and  $e_{z, p+1}^q(1, j_d, k + \frac{1}{2})$  is an unknown quantity in Eq. (19). In order to solve this problem,  $e_{z, p+1}^q$  is obtained by the process of Eq. (12) to Eq. (13a-1) iteration, and then, the result of Eq. (13a-1) is used to replace  $e_{z, p+1}^q$  in the right-side of Eq. (19). Obviously, this substitution method not only makes  $e_{z, p+1}^q$  known, but also makes it more and more accurate by cyclic iteration.

### C. ANALYSES AND DISCUSSIONS ARE ABOUT DETERMINING THE FINAL FIELDS FOR SPECIAL TREATMENT IN THE EQUATIONS

In Part B, we have explained the way about how to obtain the final special treatment scheme for on  $z$ -axis of the proposed method. It is clear that only Eq. (5a-3), Eq. (6a-1), Eq. (11a-3) and Eq. (13a-1) in the Part A and Part B of Section II need to solve  $E_z^q$ , however, it will be arbitrary and less rigorous to simply use Eq. (18) to carry out the special treatments on  $z$ -axis for the above equations.

Obviously, whether an equation needs special treatment or not depends on the existence of  $E_z^q(0, j, k + \frac{1}{2})$  (see Eq. (15b)) in the equation. Based on this, we will analyze all the equations of the proposed method in detail.

In the analyses of Figure 4, the FDTD equations of the proposed method contain  $\frac{1}{\rho}$  terms, whose denominators cannot be set as zero, arbitrarily. Therefore, the analyses of the unsolved fields for on the  $z$ -axis of all the equations in the proposed method can be divided into two cases:  $\rho = 0$  ( $i = 0, 1, 2, \dots, i_{\max} - 1$ ) and  $\rho = 1$  ( $i = 1, 2, 3, \dots, i_{\max}$ ). (1)  $\rho = 0$ ,  $E_z^q$  fields that need special treatments during the initial values and the iterative procedures are  $e_z^{q-1}(0, j, k + \frac{1}{2})$ ,  $e_z^q(0, j, k + \frac{1}{2})$ ,  $e_z^{*q}(0, j, k + \frac{1}{2})$ ,  $e_{z, p+1}^q(0, j, k + \frac{1}{2})$  and  $e_{z, p+1}^{*q}(0, j, k + \frac{1}{2})$ . (2)  $\rho = 1$ , obviously, when we make special treatments of the  $E_z^q$  fields on the  $z$ -axis, if we directly set the  $\rho$  of Eq. (5a-3), (6a-1), Eq. (11a-3) and Eq. (13a-1) to zero, this operation will inevitably lead to infinite solutions and exceed the minimum boundary (see Eq. (B.1.b) in Appendix B). Moreover, the solution processes



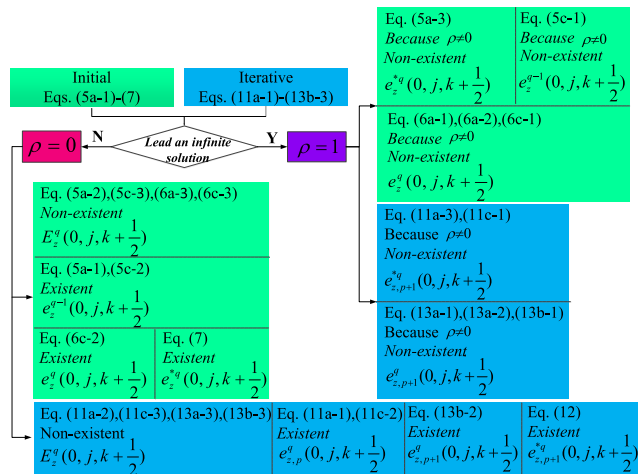


FIGURE 4. Analysis of all the equations in the proposed method on z-axis.

of some magnetic field equations are similar (see Eq. (5c-1), Eq. (6c-1), Eq. (11c-1) and Eq. (13b-1)).

**D. SPECIAL TREATMENT SCHEME WITH PROGRAMMING DESIGN ON THE FDTD DIFFERENCE IN THE  $\phi$ -DIRECTION**

As shown in Figure 5, the beginning and ending grid points of the  $\phi$ -direction on a specific plane are  $\phi = 0$  and  $\phi = \phi_{max}$ , and they are overlap, so the purpose of connecting them with periodic boundary condition is to form a closed plane. Therefore, according to the thought of cyclic matrix in [44], we combine the characteristics of FDTD spatial grid partitioning and realize the connection of the beginning and ending points in the  $\phi$ -direction by programming design, and then, forming a way which is similar to [44] for cyclic solving the fields in the  $\phi$ -direction.

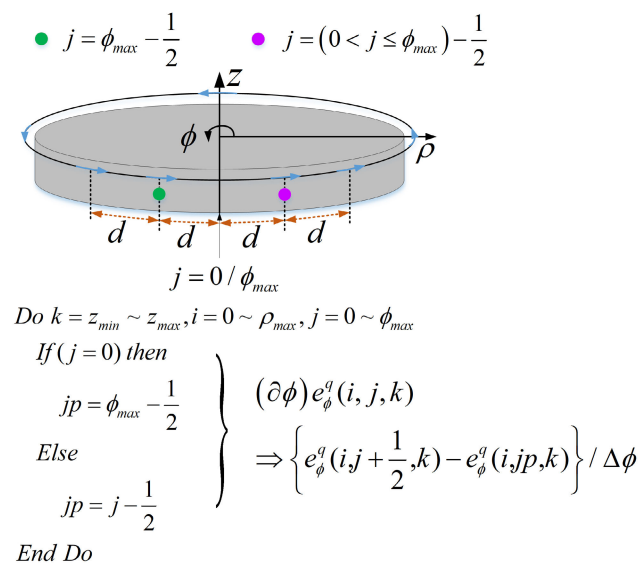


FIGURE 5. Special treatment on the  $\phi$ -direction and programming design.

In fact, the way of FDTD mesh partitioning is to realize the discrete of the fields in space by the solving relation between the integer grid point and the half grid points around the integer grid point. Therefore,  $d = \frac{1}{2}$  on the specific plane shown in Figure 5 is defined as the distance between the half grid point and the integer grid point, and at the same time,  $i, j, k$  are defined as the space grid positions in the direction of  $\rho, \phi$  and  $z$ . Obviously, when  $j = 0$ , if the grid in the  $\phi$ -direction is discretized by FDTD difference in the opposite direction ( $(j = 0) - \frac{1}{2}$ ), it will cause an out-of-boundary case, and the fields in the  $\phi$ -direction cannot form a closed ring on the specific plane. In order to solve this problem, according to the overlapping characteristics of  $j = 0$  and  $j = \phi_{max}$  in the program design, as shown in the pseudo-code of Figure 5, when  $j = 0$  and FDTD difference is carried out in the opposite direction, we can make  $j = \phi_{max}$  to maintain the calculation of periodic boundary condition in the solution process of difference discretization, and no boundary problem will occur.

To sum up, some FDTD equations of the proposed method indeed need special treatments on z-axis and  $\phi$ -direction, but it is worth noting that they need to require independent special treatments in programming, instead of simply and crude using the way of making  $\rho = 0$  and  $\phi = 0 \sim \phi_{max}$  to solve.

**IV. ANALYSES OF CONVERGENCE SPEED AND STABILITY**

Because the difference between the initial values and iterative procedures of the proposed method is the perturbation term, and the iterative procedures play a decisive role, so, we prove and discuss the stability and convergence speed with the iterative procedures as the entry point.

**A. DICUSSING THE CONVERGENCE CONDITION OF THE ITERATIVE PROCEDURES WITH MATRIX THEORY**

According to the introductions in Part B of Section II, the matrix form of the iterative procedures of the proposed method is Eq. (8). In fact, it can be evolved from the 3-D conventional cylindrical coordinate WLP-FDTD. To prove easily, we remove the excitation source in Eq. (1) here, the matrix form of the conventional WLP-FDTD in 3-D cylindrical coordinate system can be rewritten as

$$(I - A - B)W^q = V^{q-1}. \tag{20}$$

Adding  $ABW^q$  to the both sides of Eq. (20), we can obtain

$$(I - A)(I - B)W^q = ABW^q - V^{q-1}. \tag{20a}$$

By transforming Eq. (20a) into an iterative equation form, we can obtain again

$$(I - A)(I - B)W_{p+1}^q = ABW_p^q - V^{q-1}. \tag{20b}$$

Obviously, Eq. (20b) and Eq. (8) are completely consistent.

By changing the forms of Eq. (20a) and Eq. (20b), we can obtain

$$\mathbf{W}^q = \mathbf{M}^{-1}\mathbf{N}\mathbf{W}^q + \mathbf{M}^{-1}\mathbf{C} \quad (21a)$$

$$\mathbf{W}_{p+1}^q = \mathbf{M}^{-1}\mathbf{N}\mathbf{W}_p^q + \mathbf{M}^{-1}\mathbf{C} \quad (21b)$$

where  $\mathbf{M} = (\mathbf{I} - \mathbf{A})(\mathbf{I} - \mathbf{B})$ ,  $\mathbf{N} = \mathbf{A}\mathbf{B}$ ,  $\mathbf{C} = \mathbf{V}^{q-1}$ .

Here,  $\mathbf{W}^q$  is the exact solution of the  $q$ -order WLP-FDTD method, and the error of the  $p$ -th iteration is defined as

$$\mathbf{Error}_p^q = \mathbf{W}^q - \mathbf{W}_p^q. \quad (22)$$

In combination with Eq. (22), Eq. (21a) subtracts Eq. (21b), and the following equation can be obtained

$$\mathbf{Error}_{p+1}^q = \mathbf{M}^{-1}\mathbf{N}\mathbf{Error}_p^q. \quad (23)$$

According to matrix theory [45], after the  $k$ -th iteration, the relation between the error of the solution and the initial error is

$$\|\mathbf{Error}_p^q\| = \delta(\mathbf{G})^p \|\mathbf{Error}_0^q\| \quad (24)$$

where  $\|\cdot\|$  is the Euclidean norm,  $\delta(\cdot)$  is the spectral radius,  $\mathbf{Error}_0^q$  is the initial error and  $\mathbf{G} = \mathbf{M}^{-1}\mathbf{N}$ .

Obviously, Eq. (21b) conforms to the general form of a linear equation system

$$\mathbf{x}^{(k+1)} = \beta(\mathbf{G})\mathbf{x}^{(k)} + \mathbf{\Gamma} \quad (25)$$

where  $\mathbf{x}^{(k)}$  is the  $k$ -th iteration of  $\mathbf{x}$ , and at the beginning,  $k = 0$ . When  $k = 0$ ,  $\mathbf{x}^{(0)}$  is actually the  $\mathbf{Error}_0^q$  in Eq. (24),  $\beta(\mathbf{G})$  is a spectral radius,  $\mathbf{\Gamma}$  is a known column vector.

Once again, according to Jordan canonical form [46] in matrix theory, whether a linear equation system converges or not is independent of the initial error  $\mathbf{Error}_0^q$  and  $\mathbf{\Gamma}$ , but only depends on  $\beta(\mathbf{G})$ , that is, when  $\beta(\mathbf{G}) < 1$ , the iterative linear equation system is convergent. Therefore, in order to prove that the proposed method is convergent, we must prove that  $\delta(\mathbf{G}) < 1$  or the eigenvalue of the  $\mathbf{G}$  matrix is less than one (see Eq. (21b) and Eq. (24)).

### B. TRANSFORMATION OF SPECTRAL RADIUS

The coefficient matrices of the proposed method have been shown in Part A of Section II, Eq. (9a) and Eq. (9b) are the initial iteration equations after adding the non-physical intermediate variables. By simply substituting the coefficient matrices into Eq. (9a) and Eq. (9b), and removing the excitation source terms and  $V^{q-1}$  terms [28], we can obtain

$$e_\rho^{*q} + a\partial z h_\phi^{*q} = a\frac{1}{\rho}\partial\phi h_{z,p}^q \quad (26a)$$

$$e_\phi^{*q} + a\partial\rho h_z^{*q} = a\partial z h_{\rho,p}^q \quad (26b)$$

$$e_z^{*q} + a\frac{1}{\rho}\partial\phi h_\rho^{*q} = a(\frac{1}{\rho}\partial\rho)h_{\phi,p}^q \quad (26c)$$

$$h_\rho^{*q} + b\frac{1}{\rho}\partial\phi e_z^{*q} = b\partial z e_{\phi,p}^q \quad (26d)$$

$$h_\phi^{*q} + b\partial z e_\rho^{*q} = b\partial\rho e_{z,p}^q \quad (26e)$$

$$h_z^{*q} + b(\frac{1}{\rho}\partial\rho)e_\phi^{*q} = b\frac{1}{\rho}\partial\phi e_{\rho,p}^q \quad (26f)$$

$$e_{\rho,p+1}^q - a\frac{1}{\rho}\partial\phi h_{z,p+1}^q = -a\partial z h_\phi^{*q} \quad (27a)$$

$$e_{\phi,p+1}^q - a\partial z h_{\rho,p+1}^q = -a\partial\rho h_z^{*q} \quad (27b)$$

$$e_{z,p+1}^q - a(\frac{1}{\rho}\partial\rho)h_{\phi,p+1}^q = -a\frac{1}{\rho}\partial\phi h_\rho^{*q} \quad (27c)$$

$$h_{\rho,p+1}^q - b\partial z e_{\phi,p+1}^q = -b\frac{1}{\rho}\partial\phi e_z^{*q} \quad (27d)$$

$$h_{\phi,p+1}^q - b\partial\rho e_{z,p+1}^q = -b\partial z e_\rho^{*q} \quad (27e)$$

$$h_{z,p+1}^q - b\frac{1}{\rho}\partial\phi e_{\rho,p+1}^q = -b(\frac{1}{\rho}\partial\rho)e_\phi^{*q}. \quad (27f)$$

Defining  $\tilde{e}_\phi = \rho e_\phi$  and  $\tilde{h}_\phi = \rho h_\phi$ , we can rewrite Eq. (9a) and Eq. (9b) as

$$(\mathbf{I} - \mathbf{A}')\mathbf{W}^{*q'} = \mathbf{B}'\mathbf{W}^{q'} \quad (28a)$$

$$(\mathbf{I} - \mathbf{B}')\mathbf{W}^{q'} = \mathbf{A}'\mathbf{W}^{*q'} \quad (28b)$$

where

$$\mathbf{W}^{*q'} = [e_\rho^{*q} \tilde{e}_\phi^{*q} e_z^{*q} h_\rho^{*q} \tilde{h}_\phi^{*q} h_z^{*q}]^T,$$

$$\mathbf{W}^{q'} = [e_\rho^q \tilde{e}_\phi^q e_z^q h_\rho^q \tilde{h}_\phi^q h_z^q]^T,$$

$$\mathbf{A}' = \begin{bmatrix} 0 & \mathbf{A}'_{\mu\chi} \\ \mathbf{A}'_{\varepsilon\chi} & 0 \end{bmatrix}, \quad \mathbf{B}' = \begin{bmatrix} 0 & \mathbf{B}'_{\mu\chi} \\ \mathbf{B}'_{\varepsilon\chi} & 0 \end{bmatrix},$$

$$\mathbf{A}'_{\mu\chi} = \begin{bmatrix} 0 & -a\frac{1}{\rho}\partial z & 0 \\ 0 & 0 & -a\rho\partial\rho \\ -a(\frac{1}{\rho}\partial\phi) & 0 & 0 \end{bmatrix},$$

$$\mathbf{A}'_{\varepsilon\chi} = \begin{bmatrix} 0 & 0 & -b(\frac{1}{\rho}\partial\phi) \\ -b\rho\partial z & 0 & 0 \\ 0 & -b(\frac{1}{\rho}\partial\rho) & 0 \end{bmatrix},$$

$$\mathbf{B}'_{\mu\chi} = \begin{bmatrix} 0 & 0 & a(\frac{1}{\rho}\partial\phi) \\ a\rho\partial z & 0 & 0 \\ 0 & a(\frac{1}{\rho}\partial\rho) & 0 \end{bmatrix},$$

$$\mathbf{B}'_{\varepsilon\chi} = \begin{bmatrix} 0 & b\frac{1}{\rho}\partial z & 0 \\ 0 & 0 & b\rho\partial\rho \\ b(\frac{1}{\rho}\partial\phi) & 0 & 0 \end{bmatrix}.$$

In a 3-D cylindrical coordinate system, the spectral domain expressions of the electric- and the magnetic- fields can be written as

$$E_\rho^q = e_\rho^q f(\rho, \phi, z) \quad (29a)$$

$$\tilde{E}_\phi^q = \rho e_\phi^q f(\rho, \phi, z) \quad (29b)$$

$$E_z^q = e_z^q f(\rho, \phi, z) \quad (29c)$$

$$H_\rho^q = h_\rho^q f(\rho, \phi, z) \quad (29d)$$

$$\tilde{H}_\phi^q = \rho h_\phi^q f(\rho, \phi, z) \tag{29e}$$

$$H_z^q = h_z^q f(\rho, \phi, z) \tag{29f}$$

where  $f(\rho, \phi, z) = B_m(K_\rho \rho) e^{\vec{j} K_\phi \phi} e^{\vec{j} K_z z}$ ,  $\vec{j} = \sqrt{-1}$ ,  $B_m$  is the appropriate Bessel function.  $K_\rho$ ,  $K_\phi$  and  $K_z$  are the spatial frequencies along the  $\rho$ -,  $\phi$ - and  $z$ -directions, respectively.

Clearly, there are  $a$  and  $b$  in the coefficient matrices  $A'$  and  $B'$ , and they are not uniform, which will bring some troubles to the proof. Therefore, in order to normalize  $a$  and  $b$ , we're going to convert the forms of the electric- and the magnetic- fields into  $e_{\rho, \phi, z}^{q'} = e_{\rho, \phi, z}^{q''}$  and  $h_{\rho, \phi, z}^{q'} = \sqrt{\frac{\mu}{\epsilon}} h_{\rho, \phi, z}^{q''}$ , and substituting them into Eq. (28a) and Eq. (28b), we can obtain  $a = b = \Upsilon = 2c/s$  ( $c = 1/\sqrt{\epsilon\mu}$ ).

And then, we can obtain the new forms of  $A'$  and  $B'$  as

$$\ddot{A} = \begin{bmatrix} & & & 0 & -j\frac{1}{\rho}\Lambda_z & 0 \\ & 0 & & 0 & 0 & -\rho\Lambda_\rho \\ & & & -j\frac{1}{\rho}\Lambda_\phi & 0 & 0 \\ 0 & 0 & -j\frac{1}{\rho}\Lambda_\phi & & & \\ -j\rho\Lambda_z & 0 & 0 & & & 0 \\ 0 & -\frac{1}{\rho}\Lambda_\rho & 0 & & & \end{bmatrix} \tag{30a}$$

$$\ddot{B} = \begin{bmatrix} & & & 0 & 0 & j\frac{1}{\rho}\Lambda_\phi \\ & 0 & j\rho\Lambda_z & 0 & 0 & \\ & & 0 & \frac{1}{\rho}\Lambda_\rho & 0 & \\ 0 & j\frac{1}{\rho}\Lambda_z & 0 & & & \\ 0 & 0 & \rho\Lambda_\rho & & & 0 \\ j\frac{1}{\rho}\Lambda_\phi & 0 & 0 & & & \end{bmatrix} \tag{30b}$$

where  $\Lambda_\rho = \Upsilon(B_m^{\rho+\frac{1}{2}} - B_m^{\rho-\frac{1}{2}})$ ,  $\Lambda_\phi = 2\Upsilon \frac{\sin(K_\phi \frac{\Delta\phi}{2})}{\Delta\phi}$ ,  $\Lambda_z = 2\Upsilon \frac{\sin(K_z \frac{\Delta z}{2})}{\Delta z}$  (see the way of Eq. (23) in [41]).

### C. PROOF OF STABILITY AND CONVERGENCE SPEED

According to the discussions in Part A of this section, the iteration matrix of the proposed method is actually that

$$G = (I - \ddot{B})^{-1}(I - \ddot{A})^{-1}\ddot{A}\ddot{B}. \tag{31}$$

As long as the eigenvalue  $|\lambda_G| < 1$  of the matrix  $G$ , then the iterative equation Eq. (20b) is convergent. Therefore, we convert the form of Eq. (31) as

$$G = (I - \ddot{B})^{-1} [f(\ddot{A})f(\ddot{B})] (I - \ddot{B}) \tag{32}$$

where  $f(\ddot{A}) = (I - \ddot{A})^{-1}\ddot{A}$ ,  $f(\ddot{B}) = (I - \ddot{B})^{-1}\ddot{B}$ .

Obviously,  $G$  matrix and  $f(\ddot{A})f(\ddot{B})$  are similar matrices, and their eigenvalues are the same. According to matrix theory [45], the eigenvalue  $\lambda_G$  should satisfy as

$$\|\lambda_G\| \leq \|f(\ddot{A})f(\ddot{B})\| \leq \|f(\ddot{A})\| \|f(\ddot{B})\|. \tag{33}$$

Matrix theory tell us that

$$\|f(\ddot{A})\|^2 = \lambda(f(\ddot{A})f(\ddot{A})^H)_{\max} \tag{34}$$

where  $f(\ddot{A})^H$  is the conjugate transpose of  $f(\ddot{A})$ ,  $\lambda_{\max}$  is the eigenvalue of  $f(\ddot{A})f(\ddot{A})^H$ .

Here, using spectral transformation matrices Eq. (30a) and Eq. (30b), by MATLAB calculation, we can obtain

$$|\lambda_{\ddot{A}-1,5}| = \frac{\Lambda_z^2}{(\Lambda_z + 1)^2} \tag{35a}$$

$$|\lambda_{\ddot{A}-2,6}| = \frac{\Lambda_\phi^2}{(\Lambda_\phi + \rho)^2} \tag{35b}$$

$$|\lambda_{\ddot{A}-3,4}| = \frac{\Lambda_\rho^2}{(\Lambda_\rho + 1)^2}. \tag{35c}$$

Clearly,  $|\lambda_{\ddot{A}-(1-6)}| < 1$ , it can turn out that  $\|f(\ddot{A})\| < 1$ . Similarly, we can obtain

$$|\lambda_{\ddot{B}-1,5}| = \frac{\Lambda_z^2}{(\Lambda_z + 1)^2} \tag{36a}$$

$$|\lambda_{\ddot{B}-2,6}| = \frac{\Lambda_\phi^2}{(\Lambda_\phi + \rho)^2} \tag{36b}$$

$$|\lambda_{\ddot{B}-3,4}| = \frac{\Lambda_\rho^2}{(\Lambda_\rho + 1)^2}. \tag{36c}$$

The results of Eq. (36) confirm that  $|\lambda_{\ddot{B}-(1-6)}| < 1$ , namely, it also can turn out that  $\|f(\ddot{B})\| < 1$ .

By combining the conclusions of Eq. (35) and Eq. (36),  $\|\lambda_G\| < 1$  can be confirmed, that is, the proposed method is stable.

Observing Eq. (25) and Eq. (32) again, combining with the characteristic of Jordan Canonical Form in matrix theory [45], we know that  $\beta(G) \leq \|G\|$ , when  $\|G\|$  is small,  $\beta(G)$  will be smaller, then, the convergence speed of iterative method for linear equation will be faster. Therefore, if we want to prove which method converges faster, it just has to prove whose  $\beta(G)$  is smaller.

In order to prove that the convergence speed of the proposed method is faster, we make a comparison between the iterative scheme in reference [39] (in 3-D case) and the proposed one.

The iterative procedure equations in reference [39], which are similar with Eq. (9a) and Eq. (9b) in the proposed method, are given as follows (see Eq. (24) and Eq. (25) in [39])

$$(I - A)W_{p+1}^{*q} = BW_p^q + V^{q-1} \tag{37a}$$

$$(I - B)W_{p+1}^q = W_{p+1}^{*q} - BW_p^q. \tag{37b}$$

Obviously, Eq. (37a) and Eq. (9a) are identical. Therefore, by comparing the eigenvalues of Eq. (37b) and Eq. (9b), we can prove which method has the faster convergence speed. As discussed in Part A and Part B of this section, because  $W_p^q$ ,  $W_{p+1}^{*q}$  and  $V^{q-1}$  are the known values of both methods, so,

we can approximately transform Eq. (37b) and Eq. (9b) as the form of Eq. (25)

$$\mathbf{W}_{1,p+1}^q = (\mathbf{I} - \check{\mathbf{B}})^{-1} \mathbf{W}_{1,p+1}^{*q} + \mathbf{\Gamma}_1 \quad (38a)$$

$$\mathbf{W}_{2,p+1}^q = (\mathbf{I} - \check{\mathbf{B}})^{-1} \check{\mathbf{A}} \mathbf{W}_{2,p+1}^{*q} + \mathbf{\Gamma}_2. \quad (38b)$$

where,  $\mathbf{\Gamma}_1$  and  $\mathbf{\Gamma}_2$  are the known values of both method.

According to the conclusions above, we can know that  $\beta(\mathbf{G}_1) = (\mathbf{I} - \check{\mathbf{B}})^{-1}$  and  $\beta(\mathbf{G}_2) = (\mathbf{I} - \check{\mathbf{B}})^{-1} \check{\mathbf{A}}$ . By MATLAB calculation, we can obtain the similar results.

$$|\lambda_{G_1-1,4}| = (\Lambda_\rho + 1)^2, \quad (39a)$$

$$|\lambda_{G_1-2,3}| = (\Lambda_z + 1)^2, \quad (39b)$$

$$|\lambda_{G_1-5,6}| = \frac{(\Lambda_\phi + \rho)^2}{\rho^2}, \quad (39c)$$

$$|\lambda_{G_2-1,4}| = \frac{(\Lambda_\rho + 1)^2}{\Lambda_\rho^2} \quad (40a)$$

$$|\lambda_{G_2-2,3}| = \frac{(\Lambda_z + 1)^2}{\Lambda_z^2} \quad (40b)$$

$$|\lambda_{G_2-5,6}| = \frac{(\Lambda_\phi + \rho)^2}{\Lambda_\phi^2} \quad (40c)$$

By comparing Eq. (39) and Eq. (40), it is obvious that  $\|\mathbf{G}_2\| < \|\mathbf{G}_1\|$ , namely,  $\beta(\mathbf{G}_2) < \beta(\mathbf{G}_1)$ . In other words, the convergence speed of the proposed method is faster than that in reference [39].

To sum up, the proposed method combines the ADI linear iteration which eliminates the CFL [37] and the WLP scheme which eliminates the time  $\Delta t$  [40], it makes the advantages of the proposed method at stability and convergence speed.

### V. DISCUSSIONS OF THE CHOICE SCHEMES OF PARAMETERS

In a Laguerre-based FDTD method, the choice scheme in the term of time-scaling factor  $s$  and the highest expansion order of the weighted Laguerre polynomials  $q$  has a great influence on the accuracy of numerical calculation. There is still no unified conclusion on how to choose the optimal parameter. In this paper, the choice schemes of  $s$  and  $q$  parameters will refer to the method in reference [47].

For any time-domain method, it can be expanded by the Laguerre function as

$$\mathfrak{R}(t) = \sum_{\vartheta}^{\infty} c_{\vartheta} \varphi_{\vartheta}(st) \quad (41)$$

where,  $\mathfrak{R}(t)$  is an arbitrary transient function,  $s$  is a time-scaling factor, and  $\varphi_{\vartheta}(st)$  is the Laguerre polynomial of the  $\vartheta$ -th degree.  $s$  is needed because of the duration of a transient process usually depends on the type of problem, and it can vary widely from nanoseconds to several hundred nanoseconds [40], [47]. If there is no  $s$ , the value of the Laguerre function is very close to  $\varphi_{\vartheta}(0)$ , and it is not suitable for expansion of the transient response. Eq. (41) is a theoretical

formula, but for practical problems, it can only use a finite number of degrees to expand a function

$$\mathfrak{R}(t) = \sum c_{\vartheta} \varphi_{\vartheta}(st). \quad (42)$$

The summation of the  $q$  terms will result in an approximate error, which is mainly related to the time-scaling factor  $s$  and the highest degree  $q-1$ . Therefore, how to choose  $s$  and  $q$  is particularly important.

As discussed in [47], we can define the error as

$$\mathfrak{S}_q^2 = \frac{1}{\|\mathfrak{R}\|^2} \int_0^{\infty} \left( \mathfrak{R}(t) - \sum c_{\vartheta} \varphi_{\vartheta}(st) \right)^2 dt = \frac{1}{s \|\mathfrak{R}\|^2} \sum_{\vartheta=q}^{\infty} c_{\vartheta}^2 \quad (43)$$

where  $\|\mathfrak{R}\|^2 = \int_0^{\infty} \mathfrak{R}^2(t) dt = \left(\frac{1}{s}\right) \sum_{\vartheta=0}^{\infty} c_{\vartheta}^2$ .

If defining

$$m_1 = \frac{1}{\|\mathfrak{R}\|^2} \int_0^{\infty} t \mathfrak{R}^2(t) dt \quad (44a)$$

$$m_2 = \frac{1}{\|\mathfrak{R}\|^2} \int_0^{\infty} t \left( \frac{d}{dt} \mathfrak{R}(t) \right)^2 dt \quad (44b)$$

then, for any function that belongs to the following set

$$\Phi = \left( \mathfrak{R} : \frac{1}{\|\mathfrak{R}\|^2} \int_0^{\infty} t \mathfrak{R}^2(t) dt = m_1, \frac{1}{\|\mathfrak{R}\|^2} \int_0^{\infty} t \left( \frac{d}{dt} \mathfrak{R}(t) \right)^2 dt = m_2 \right) \quad (45)$$

there is

$$\max_{\mathfrak{R} \in \Phi} \mathfrak{S}_q^2 \leq \frac{s^2 m_1 + 4m_2 - 2s}{4sq}. \quad (46)$$

Eq. (46) gives an upper limit of error  $\mathfrak{S}_q^2$ , and it is a minimum upper limit [47]. Obviously, this minimum upper limit is closely related to the time-scaling factor  $s$  and the highest order of expansion  $q$ . The error  $\mathfrak{S}_q^2$  can be reduced by increasing the highest expansion order  $q$  or selecting the appropriate  $s$ . According to the partial differential processing method in reference [47], the optimal time-scaling factor can be obtained as

$$s_{opt} = \sqrt{\frac{4m_2}{m_1}}. \quad (47)$$

In Eq. (47), it should be explained that this optimal time-scaling factor is obtained in the sense of minimizing the upper bound of the error, not minimizing the error, still, it is great significant. When the method itself and the structural parameters of the scatterer are not taken into account, its general value range is  $s_{opt}/5 \leq s \leq 5s_{opt}$  [47].

Here, we use the modulated Gaussian excitation source as an example to verify. The excitation source is given as follow

$$E_i(t) = E_0 \cos(2\pi f_0 t) e^{-4\pi((t-t_0)/\tau)^2} \quad (48)$$

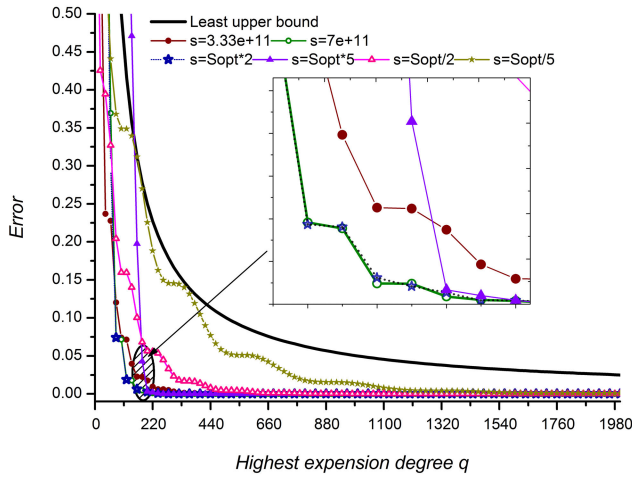


**FIGURE 6.** Variations of the error with the highest expansion order when selecting different time-scaling factors.

where  $E_0 = 10^3$  V/m,  $f_0 = 10$  GHz,  $\tau = 1.0/f_0$  and  $t_0 = 1.25/f_0$ .

By MATLAB calculation,  $m_1 = 1.8e - 11$  and  $m_2 = 5.0e + 11$  can be obtained, and then the optimal time-scaling factor can be obtained by Eq. (47) as  $3.33e + 11$ .

Figure 6 shows the variations of the error  $\mathfrak{S}_q^2$  with the highest expansion order  $q$  when selecting different time-scaling factors. Where, the curve marked “Least upper bound” represents the upper limit of the minimum error of the function set. Obviously, when the excitation source selection conforms to the situation of Eq. (48), the proposed method in this paper should be properly adjusted in the range of  $s = 7e + 11$  and  $q = 100 \sim 220$ .

It is worth noting that the premise of the choice schemes of  $s$  and  $q$  discussed is not affected by factors such as the method itself and the structural parameters of the scatterer. Although there is no final and unified conclusion on the optimal selection of  $s$  and  $q$  in the research field [47], these factors have to be considered and discussed in the numerical simulation of the following paper. Therefore, there may be slightly deviated about the final  $s$  and  $q$  of the proposed method, this does not mean that we should ignore the choices of  $s$  and  $q$ . On the contrary, we should determine their rang in advance, so that we can locate the factors that affect the accuracy as soon as possible in the verification of future numerical simulation examples, rather than blindly trying many times.

## VI. PML IMPLEMENTATION FOR THE PROPOSED METHOD

To reduce the reflection of the outer boundary and prove the advantage of the accuracy of the proposed method, we develop the PML implementation for the proposed method.

### A. PML IMPLEMENTATION OF THE CONVENTIONAL FDTD METHOD BASED ON STRETCHING COORDINATE TRANSFORMATION IN 3-D CYLINDRICAL COORDINATE SYSTEM

As described in [9], the achieved PML of FDTD method through the transformation of stretching coordinates in the frequency-domain. Therefore, the following introductions will begin with the frequency-domain forms of the FDTD method in 3-D cylindrical coordinate system.

We can directly obtain the frequency-domain forms of Eq. (3) and Eq. (5) in [48] as

$$-j\omega\mu H_\rho = \frac{1}{\tilde{\rho}} \frac{\partial E_z}{\partial \phi} - \frac{\partial E_\phi}{\partial \tilde{z}} - M_{h\rho} \quad (49a)$$

$$-j\omega\mu H_\phi = \frac{\partial E_\rho}{\partial \tilde{z}} - \frac{\partial E_z}{\partial \tilde{\rho}} - M_{h\phi} \quad (49b)$$

$$-j\omega\mu H_z = \frac{1}{\tilde{\rho}} \frac{\partial(\tilde{\rho}E_\phi)}{\partial \tilde{\rho}} - \frac{1}{\tilde{\rho}} \frac{\partial E_\rho}{\partial \phi} - M_{hz} \quad (49c)$$

$$j\omega\varepsilon E_\rho = \frac{1}{\tilde{\rho}} \frac{\partial H_z}{\partial \phi} - \frac{\partial H_\phi}{\partial \tilde{z}} - J_{e\rho} \quad (49d)$$

$$j\omega\varepsilon E_\phi = \frac{\partial H_\rho}{\partial \tilde{z}} - \frac{\partial H_z}{\partial \tilde{\rho}} - J_{e\phi} \quad (49e)$$

$$j\omega\varepsilon E_z = \frac{1}{\tilde{\rho}} \frac{\partial(\tilde{\rho}H_\phi)}{\partial \tilde{\rho}} - \frac{1}{\tilde{\rho}} \frac{\partial H_\rho}{\partial \phi} - J_{ez} \quad (49f)$$

where  $[J_{e\rho}^q, J_{e\phi}^q, J_{ez}^q, M_{h\rho}^q, M_{h\phi}^q, M_{hz}^q]^T$  is the excitation source,  $\tilde{\rho}$  and  $\tilde{z}$  represent the results of the transformation of stretching coordinates, and  $\varepsilon$ ,  $\mu$  and  $\partial_l$  are same as above.

The formulations of the transformation of stretching coordinates can be given as

$$\tilde{\rho} = \rho_0 + \int_{\rho_0}^{\rho} \xi_\rho(\rho') d\rho' \quad (50a)$$

$$\tilde{z} = z_0 + \int_{z_0}^z \xi_z(z') dz' \quad (50b)$$

in which  $\rho_0$  and  $z_0$  are the inner boundaries of the matched layer,  $\xi_l$  ( $l = \rho, \phi, z$ ) is the coefficient of stretching transformation.

Obviously, Eq. (49a) to Eq. (49f) must be transformed into the forms with the parameter  $\xi_l$  of stretching transformation in order to perform PML transformation of the FDTD method. Therefore, we define

$$\xi_\rho(\rho) = \xi_\rho \quad (51a)$$

$$\frac{\tilde{\rho}}{\rho} = \xi_\phi(\rho) = \xi_\phi \quad (51b)$$

$$\xi_z(z) = \xi_z. \quad (51c)$$

In fact,  $\xi_\rho$  and  $\xi_z$  are given by taking the derivatives for  $\tilde{\rho}$  and  $\tilde{z}$ . At the same time, because the directions of the fields in the  $\phi$ -direction are uncertain, they do not participate in the transformation of stretching coordinates.

The detailed methods for obtaining Eq. (51a) to Eq. (51c) are shown in Appendix C.



Furthermore, Eq. (51a) to Eq. (51c) are substituted into the group of Eq. (49a) to Eq. (49f), we can obtain the basic equations of PML, which are derived from 3-D conventional cylindrical coordinate FDTD method. They are given as

$$-j\omega\mu H_\rho = \frac{1}{\rho} \frac{1}{\xi_\phi} \frac{\partial E_z}{\partial \phi} - \frac{1}{\xi_z} \frac{\partial E_\phi}{\partial z} - M_{h\rho} \quad (52a)$$

$$-j\omega\mu H_\phi = \frac{1}{\xi_z} \frac{\partial E_\rho}{\partial z} - \frac{1}{\xi_\rho} \frac{\partial E_z}{\partial \rho} - M_{h\phi} \quad (52b)$$

$$-j\omega\mu H_z = \frac{1}{\xi_\rho} \frac{\partial E_\phi}{\partial \rho} + \frac{1}{\xi_\phi} \frac{1}{\rho} E_\phi - \frac{1}{\rho} \frac{1}{\xi_\phi} \frac{\partial E_\rho}{\partial \phi} - M_{hz} \quad (52c)$$

$$j\omega\varepsilon E_\rho = \frac{1}{\rho} \frac{1}{\xi_\phi} \frac{\partial H_z}{\partial \phi} - \frac{1}{\xi_z} \frac{\partial H_\phi}{\partial z} - J_{e\rho} \quad (52d)$$

$$j\omega\varepsilon E_\phi = \frac{1}{\xi_z} \frac{\partial H_\rho}{\partial z} - \frac{1}{\xi_\rho} \frac{\partial H_z}{\partial \rho} - J_{e\phi} \quad (52e)$$

$$j\omega\varepsilon E_z = \frac{1}{\xi_\rho} \frac{\partial H_\phi}{\partial \rho} + \frac{1}{\xi_\phi} \frac{1}{\rho} H_\phi - \frac{1}{\rho} \frac{1}{\xi_\phi} \frac{\partial H_\rho}{\partial \phi} - J_{ez}. \quad (52f)$$

### B. PML IMPLEMENTATION OF THE CONVENTIONAL WLP-FDTD METHOD IN 3-D CYLINDRICAL COORDINATE SYSTEM

As discussed in many WLP-FDTD methods [30], [31], [32], [40], the WLP-FDTD is actually by transforming the time-domain problems of the FDTD method to the Laguerre-domain using the Galerkin's testing procedure. The general form of the transformation equation is

$$\frac{\partial U(\mathbf{r}, t)}{\partial t} = s \sum_{q=0}^{\infty} \left( \frac{1}{2} U_q(\mathbf{r}) + \sum U_\vartheta(\mathbf{r}) \right) \Phi_q(\bar{t}) \quad (53)$$

where  $\Phi_q(\bar{t})$  is the Laguerre polynomial with weight  $e^{-\bar{t}/2}$ , and  $\bar{t}$  is the time of scaling, and  $U(\mathbf{r}, t)$  is any field quantity from the group of Eq. (49a) to Eq. (49f). According to the property of Laguerre polynomial, Eq. (53) represents the first partial derivative of  $U(\mathbf{r}, t)$  with respect to time  $t$ .

Nevertheless, if we expand the group of Eq. (52a) to Eq. (52f) by directly applying Eq. (53), we can obtain the PML implementation of WLP-FDTD, but it is still a 3-D one. Since the PML parameters are more complex, they can cause large memory consumption [48], and the Laguerre function itself can cause some memory consumption [30]. The combination of them may lead greater memory consumption for the computation of the PML implementation of WLP-FDTD. In order to solve this problem, we adopt the split-field technique [49] to convert the 3-D PML implementation to the 2-D problem for calculation.

Here, the PML scheme in [50] is applied with

$$\xi_l = \kappa_l + \frac{\sigma_l}{j\omega\varepsilon_0} \quad (l = \rho, \phi, z). \quad (54)$$

where  $\kappa_l$  and  $\sigma_l$  are the parameters of matched layer,  $\varepsilon_0$  is the permittivity without dielectric.

By substituting Eq. (54) into Eq. (52a), the difference between whether to use the split-field technique or not can be found.

If we use the split-field technique, we can obtain

$$\kappa_\phi \frac{\partial H_{\rho\phi}}{\partial t} + \frac{\sigma_\phi}{\varepsilon_0} H_{\rho\phi} = -\frac{1}{\mu} \frac{1}{\rho} \frac{\partial E_z}{\partial \phi} + \xi_\phi \frac{1}{\mu} M_{\rho\phi} \quad (55a)$$

$$\kappa_z \frac{\partial H_{\rho z}}{\partial t} + \frac{\sigma_z}{\varepsilon_0} H_{\rho z} = \frac{1}{\mu} \frac{\partial E_\phi}{\partial z} + \xi_z \frac{1}{\mu} M_{\rho z} \quad (55b)$$

where  $H_\rho = H_{\rho\phi} + H_{\rho z}$ ,  $M_\rho = M_{\rho\phi} + M_{\rho z}$ .

Obviously, comparing the term of Eq. (55a) and Eq. (55b) with Eq. (52a), it can be found that the new field components of the right-side of Eq. (55a) and Eq. (55b) are only in  $\phi$ - and  $z$ -directions. If they are taken as solving variables, 2-D field equations can be derived, which can transform 3-D problems into 2-D problems for solving, thus effectively reducing memory and saving computation time. The derivations of other equations are similar to Eq. (55a) and Eq. (55b), which will not be described here.

Here, we treat the group of Eq. (52a) to Eq. (52f) by referring to the split-field expansions of Eq. (55a) and Eq. (55b), and integrate them through mathematical operations. The PML implementation equations of the conventional WLP-FDTD method in 3-D cylindrical coordinate system can be written as

$$\begin{aligned} h_\rho^q &= h_{\rho z}^q + h_{\rho\phi}^q \\ &= N_z \left( \frac{b}{\kappa_z} \frac{\partial e_\phi^q}{\partial z} - 2 \sum h_{\rho z}^\vartheta \right) - N_\phi \left( \frac{b}{\rho\kappa_\phi} \frac{\partial e_z^q}{\partial \phi} + 2 \sum h_{\rho\phi}^\vartheta \right) \\ &\quad + \left( \frac{bN_z \xi_z}{\kappa_z} M_{\rho z}^q + \frac{bN_\phi \xi_\phi}{\kappa_\phi} M_{\rho\phi}^q \right) \end{aligned} \quad (56a)$$

$$\begin{aligned} h_\phi^q &= h_{\phi\rho}^q + h_{\phi z}^q \\ &= N_\rho \left( \frac{b}{\kappa_\rho} \frac{\partial e_z^q}{\partial \rho} - 2 \sum h_{\phi\rho}^\vartheta \right) - N_z \left( \frac{b}{\kappa_z} \frac{\partial e_\rho^q}{\partial z} + 2 \sum h_{\phi z}^\vartheta \right) \\ &\quad + \left( \frac{bN_\rho \xi_\rho}{\kappa_\rho} M_{\phi\rho}^q + \frac{bN_z \xi_z}{\kappa_z} M_{\phi z}^q \right) \end{aligned} \quad (56b)$$

$$\begin{aligned} h_z^q &= h_{z\phi}^q + h_{z\rho}^q \\ &= N_\phi \left( \frac{-b}{\rho\kappa_\phi} \left( e_\phi^q - \frac{\partial e_\rho^q}{\partial \phi} \right) \right) - N_\rho \left( \frac{b}{\kappa_\rho} \frac{\partial e_\phi^q}{\partial \rho} + 2 \sum h_{z\rho}^\vartheta \right) \\ &\quad + \left( \frac{bN_\phi \xi_\phi}{\kappa_\phi} M_{z\phi}^q + \frac{bN_\rho \xi_\rho}{\kappa_\rho} M_{z\rho}^q \right) \end{aligned} \quad (56c)$$

$$\begin{aligned} e_\rho^q &= e_{\rho\phi}^q + e_{\rho z}^q \\ &= N_\phi \left( \frac{a}{\rho\kappa_\phi} \frac{\partial h_z^q}{\partial \phi} - 2 \sum e_{\rho\phi}^\vartheta \right) - N_z \left( \frac{a}{\kappa_z} \frac{\partial h_\phi^q}{\partial z} + 2 \sum e_{\rho z}^\vartheta \right) \\ &\quad + \left( \frac{aN_\phi \xi_\phi}{\kappa_\phi} J_{\rho\phi}^q + \frac{aN_z \xi_z}{\kappa_z} J_{\rho z}^q \right) \end{aligned} \quad (56d)$$

$$\begin{aligned} e_\phi^q &= e_{\phi z}^q + e_{\phi\rho}^q \\ &= N_z \left( \frac{a}{\kappa_z} \frac{\partial h_\rho^q}{\partial z} - 2 \sum e_{\phi z}^\vartheta \right) - N_\rho \left( \frac{a}{\kappa_\rho} \frac{\partial h_z^q}{\partial \rho} + 2 \sum e_{\phi\rho}^\vartheta \right) \\ &\quad + \left( \frac{aN_z \xi_z}{\kappa_z} J_{\phi z}^q + \frac{aN_\rho \xi_\rho}{\kappa_\rho} J_{\phi\rho}^q \right) \end{aligned} \quad (56e)$$

$$\begin{aligned}
 e_z^q &= e_{z\rho}^q + e_{z\phi}^q \\
 &= N_\rho \left( \frac{a}{\kappa_\rho} \frac{\partial h_\phi^q}{\partial \rho} - 2 \sum e_{z\rho}^\vartheta \right) - N_\phi \left( \frac{-a}{\rho \kappa_\phi} (h_\phi^q - \frac{\partial h_\rho^q}{\partial \phi}) \right. \\
 &\quad \left. - \left( \frac{aN_\rho \xi_\rho}{\kappa_\rho} J_{z\rho}^q + \frac{aN_\phi \xi_\phi}{\kappa_\phi} J_{z\phi}^q \right) \right) \quad (56f)
 \end{aligned}$$

where  $N_i = \left(1 + \frac{2\sigma_i}{sk_i \varepsilon_0}\right)^{-1}$  ( $i = \rho, \phi, z$ ).

Observing the group of Eq. (56a) to Eq. (56f), it is obvious that, although the spatial distribution of each electromagnetic field component is 3-D, it can be updated by 2-D mode. This will bring some feasibility to the implementation of the PML.

By defining  $\mathbf{W}_{pml}^q = \begin{bmatrix} \mathbf{W}_{E-pml}^q & \mathbf{W}_{H-pml}^q \end{bmatrix}^T$ ,  $\mathbf{V}_{EH-pml}^{q-1} = \begin{bmatrix} \mathbf{V}_{E-pml}^{q-1} & \mathbf{V}_{H-pml}^{q-1} \end{bmatrix}^T$ ,  $\mathbf{R}_{JM-pml}^q = \begin{bmatrix} \mathbf{R}_{J-pml}^q & \mathbf{R}_{M-pml}^q \end{bmatrix}^T$ , we can write the PML implementation of Eq. (1) as

$$(\mathbf{I} - \mathbf{A}^{pml} - \mathbf{B}^{pml}) \mathbf{W}_{pml}^q = \mathbf{V}_{EH-pml}^{q-1} + \mathbf{R}_{JM-pml}^q. \quad (57)$$

Note that,

$$\begin{aligned}
 \mathbf{A}^{pml} &= \begin{bmatrix} 0 & \mathbf{A}_{\mu\chi}^{pml} \\ \mathbf{A}_{\varepsilon\chi}^{pml} & 0 \end{bmatrix}, \quad \mathbf{B}^{pml} = \begin{bmatrix} 0 & \mathbf{B}_{\mu\chi}^{pml} \\ \mathbf{B}_{\varepsilon\chi}^{pml} & 0 \end{bmatrix}, \\
 \mathbf{A}_{\mu\chi}^{pml} &= \begin{bmatrix} 0 & -aD_z \partial_z & 0 \\ 0 & 0 & -aD_\rho \partial_\rho \\ -\frac{a}{\rho} D_\phi \partial_\phi & 0 & 0 \end{bmatrix}, \\
 \mathbf{A}_{\varepsilon\chi}^{pml} &= \begin{bmatrix} 0 & 0 & -\frac{b}{\rho} D_\phi \partial_\phi \\ -bD_z \partial_z & 0 & 0 \\ 0 & -b \left( D_\rho \partial_\rho + \frac{1}{\rho} \partial_\phi \right) & 0 \end{bmatrix}, \\
 \mathbf{B}_{\mu\chi}^{pml} &= \begin{bmatrix} 0 & 0 & \frac{a}{\rho} D_\phi \partial_\phi \\ aD_z \partial_z & 0 & 0 \\ 0 & a \left( D_\rho \partial_\rho + \frac{1}{\rho} \partial_\phi \right) & 0 \end{bmatrix}, \\
 \mathbf{B}_{\varepsilon\chi}^{pml} &= \begin{bmatrix} 0 & bD_z \partial_z & 0 \\ 0 & 0 & bD_\rho \partial_\rho \\ \frac{b}{\rho} D_\phi \partial_\phi & 0 & 0 \end{bmatrix}, \\
 \mathbf{V}_{E-pml}^{q-1} &= \begin{bmatrix} -2N_\phi \sum e_{\rho\phi}^\vartheta - 2N_z \sum e_{\rho z}^\vartheta \\ -2N_\rho \sum e_{\phi\rho}^\vartheta - 2N_z \sum e_{\phi z}^\vartheta \\ -2N_\rho \sum e_{z\rho}^\vartheta - 2N_\phi \sum e_{z\phi}^\vartheta \end{bmatrix}, \\
 \mathbf{V}_{H-pml}^{q-1} &= \begin{bmatrix} -2N_\phi \sum h_{\rho\phi}^\vartheta - 2N_z \sum h_{\rho z}^\vartheta \\ -2N_\rho \sum h_{\phi\rho}^\vartheta - 2N_z \sum h_{\phi z}^\vartheta \\ -2N_\rho \sum h_{z\rho}^\vartheta - 2N_\phi \sum h_{z\phi}^\vartheta \end{bmatrix}, \\
 \mathbf{R}_{J-pml}^q &= \begin{bmatrix} -a \left( D_\phi \xi_\phi J_{\rho\phi}^q + D_z \xi_z J_{\rho z}^q \right) \\ -a \left( D_z \xi_z J_{\phi z}^q + D_\rho \xi_\rho J_{\phi\rho}^q \right) \\ -a \left( D_\rho \xi_\rho J_{z\rho}^q + D_\phi \xi_\phi J_{z\phi}^q \right) \end{bmatrix},
 \end{aligned}$$

$$\mathbf{R}_{M-pml}^q = \begin{bmatrix} b \left( D_\phi \xi_\phi M_{\rho\phi}^q + D_z \xi_z M_{\rho z}^q \right) \\ b \left( D_z \xi_z M_{\phi z}^q + D_\rho \xi_\rho M_{\phi\rho}^q \right) \\ b \left( D_\rho \xi_\rho M_{z\rho}^q + D_\phi \xi_\phi M_{z\phi}^q \right) \end{bmatrix},$$

where  $D_i = \frac{N_i}{\kappa_i}$  ( $i = \rho, \phi, z$ ).

It is worth explaining that all the fields in Eq. (57) have been updated by the 2-D models with the parameters of matched layer, they are not necessary to use the split-field technique again. Otherwise, this operation will cause the overlap of the calculation.

At this point, the derivation of PML implementation of the WLP-FDTD has been completed. The detailed derivation processes from Eq. (52) to Eq. (57) are shown in Appendix D.

### C. PML IMPLEMENTATION OF THE PROPOSED METHOD

Benefitting from the split-field technique using in Part B of this section, the general form of Eq. (56) is formed. Obviously, the difference between Eq. (57) and Eq. (1) is whether there are parameters of matched layer. Therefore, the coefficient matrices of Eq. (1) can be directly replaced by the new ones of Eq. (57), and then, by using the ways of the initial values and the iterative procedures to expand the PML implementation formulas of the proposed method.

For example, the coefficient matrices of Eq. (5a) are directly replaced by the new ones, we can obtain

$$\begin{aligned}
 &(\mathbf{I} - \mathbf{A}_{\mu\chi}^{pml} \mathbf{A}_{\varepsilon\chi}^{pml}) \mathbf{W}_{E-pml}^{*q} \\
 &= -\mathbf{A}_{\mu\chi}^{pml} \mathbf{B}_{\varepsilon\chi}^{pml} \mathbf{W}_{E-pml}^{q-1} + \mathbf{A}_{\mu\chi}^{pml} \mathbf{V}_{H-pml}^{q-1} + \mathbf{V}_{E-pml}^{q-1} \\
 &\quad - \mathbf{B}_{\mu\chi}^{pml} \mathbf{W}_{H-pml}^{q-1} + \mathbf{R}_{J-pml}^q + \mathbf{A}_{\mu\chi}^{pml} \mathbf{R}_{M-pml}^q \quad (58)
 \end{aligned}$$

Expanding Eq. (58) and directly use the Gauss-Seidel ideology to obtain

$$\begin{aligned}
 &(\mathbf{I} - ab(D_z \partial_z)^2) e_\rho^{*q} \\
 &= -abD_z \partial_z D_\rho \partial_\rho e_z^{q-1} + aD_\phi \frac{1}{\rho} \partial_\phi h_z^{q-1} \\
 &\quad + 2aD_z \partial_z [N_\rho \Sigma h_{\phi\rho}^\vartheta + N_z \Sigma h_{\phi z}^\vartheta] - 2[N_\phi \Sigma e_{\rho\phi}^\vartheta + N_z \Sigma e_{\rho z}^\vartheta] + \mathbf{R}_1^q \quad (58a)
 \end{aligned}$$

$$\begin{aligned}
 &(\mathbf{I} - abD_\rho \partial_\rho \left( D_\rho \partial_\rho + D_\phi \frac{1}{\rho} \right)) e_\phi^{*q} \\
 &= -abD_\rho \partial_\rho \left( D_\phi \frac{1}{\rho} \partial_\phi \right) e_\rho^{*q} + aD_z \partial_z h_\rho^{q-1} \\
 &\quad + 2aD_\rho \partial_\rho [N_\rho \Sigma h_{z\rho}^\vartheta + N_\phi \Sigma h_{z\phi}^\vartheta] - [N_\rho \Sigma e_{\phi\rho}^\vartheta + N_z \Sigma e_{\phi z}^\vartheta] + \mathbf{R}_2^q \quad (58b)
 \end{aligned}$$

$$\begin{aligned}
 &(\mathbf{I} - ab \left( D_\phi \frac{1}{\rho} \partial_\phi \right)^2) e_z^{*q} \\
 &= -abD_\phi \left( \frac{1}{\rho} \partial_\phi \right) D_z \partial_z e_\phi^{*q} + a \left( D_\rho \partial_\rho + D_\phi \frac{1}{\rho} \right) h_\phi^{q-1} \\
 &\quad + 2aD_\phi \frac{1}{\rho} \partial_\phi [N_\phi \Sigma h_{\rho\phi}^\vartheta + N_z \Sigma h_{\rho z}^\vartheta] + \mathbf{R}_3^q \quad (58c)
 \end{aligned}$$

$$\begin{aligned} & \mathbf{R}_1^q \\ &= -a \left( bD_z \partial_z \left[ F_\rho M_{\phi\rho}^q + F_z M_{\phi z}^q \right] + \left[ F_\phi J_{\rho\phi}^q + F_z J_{\rho z}^q \right] \right) \end{aligned} \quad (58a-s)$$

$$\begin{aligned} & \mathbf{R}_2^q \\ &= -a \left( bD_\rho \partial_z \left[ F_\phi M_{z\phi}^q + F_\rho M_{z\rho}^q \right] + \left[ F_z J_{\phi z}^q + F_\rho J_{\phi\rho}^q \right] \right) \end{aligned} \quad (58b-s)$$

$$\begin{aligned} & \mathbf{R}_3^q \\ &= -a \left( bD_\phi \frac{1}{\rho} \partial_\phi \left[ F_z M_{\rho z}^q + F_\phi M_{\rho\phi}^q \right] + \left[ F_\rho J_{z\rho}^q + F_\phi J_{z\phi}^q \right] \right) \end{aligned} \quad (58c-s)$$

where  $F_i = D_i \xi_i$  ( $i = \rho, \phi, z$ ).

Other PML implementation expansions of the proposed method are similar to those of Eq. (58a) to Eq. (58c), and the execution processes can be seen in Section II, which will not be described here.

### VII. NUMERICAL EXAMPLES

To demonstrate the term of efficiency and accuracy and the above discussions in the proposed method, Figure 7 shows an asymmetric scattering field structure in 3-D cylindrical coordinate system.

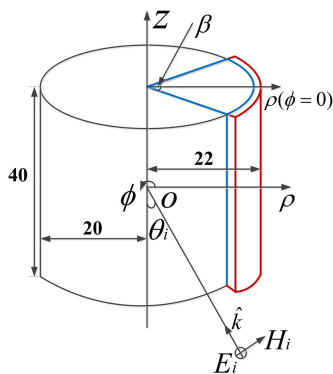


FIGURE 7. Illustration of the asymmetric structure with one wedge-shaped bulge under oblique incident wave.

As shown in Figure 7, there is one wedge-shaped bulge, the angle of the bulge is  $\beta = \frac{\pi}{4}$ . And the radius of the bulge is 22 cm, the radius and height of the cylindrical are 20 cm and 40 cm, respectively. The oblique incident plane wave is added through Huygens's surface at  $\rho = 25$  cm and  $z = \pm 25$  cm, and parallel to the  $\phi = 0$  plane, the incident angle is  $\theta_i = 45^\circ$ . The computational domain are meshed using the uniform grids with  $\Delta\rho = \Delta z = 1$  mm and  $\Delta\phi = \frac{2\pi}{40}$ , leading to the total mesh of  $40(\rho) \times 40(\phi) \times 80(z)$ , and the first order Mur absorbing boundary condition is used to truncate the boundary [51]. It should be noted that the incident electric field used in the following examples is Eq. (48) in Section V.

In the first example, how to obtain the final choices of  $s$  and  $q$  of the proposed method, we choose the observation points

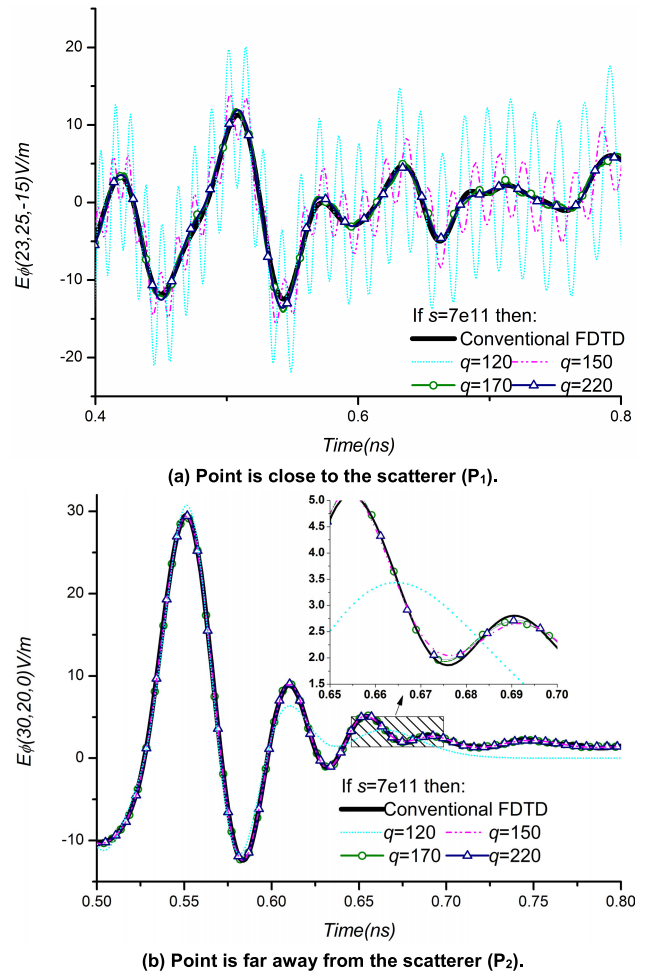


FIGURE 8. Final choices of  $s$  and  $q$  of the proposed method: (a)  $P_1$ ; (b)  $P_2$ .

$P_1$  (23, 25, -15) and  $P_2$  (30, 20, 0), which are close to and far away from the scatterer, respectively.

As shown in Figure (8a) and Figure (8b), it is obvious that when the proposed method and the structural parameters of the scatterer are taken into account, the resonance intensities of the waves are different when they are close to and far away from the scatterer. If  $s = 7e + 11$ , then  $q=170$  is the most appropriate for the proposed method. Although  $q = 150$  is selected at  $P_2$  point, and it is close to the target value, but there is still a slight deviation. In order to unify the calculation conditions,  $s = 7e + 11$  and  $q = 170$  are selected as the final choices in the proposed method.

In the second example, the importance of the special treatment for on  $z$ - axis is verified here, In this case, we're going to pick points  $P_3$  (1, 3, 23),  $P_4$  (1, 0, 25) and  $P_5$ (1, 10, 30), and they're going to have to be very close to the  $z$ - axis.

Clearly, the distances between observation points and the scatterer are different, which will make the intensity of the field transformation different and make the waveform datum more valuable for analysis.

In order to reduce the reflection error caused by the Mur absorption boundary, the 3-D conventional cylindrical

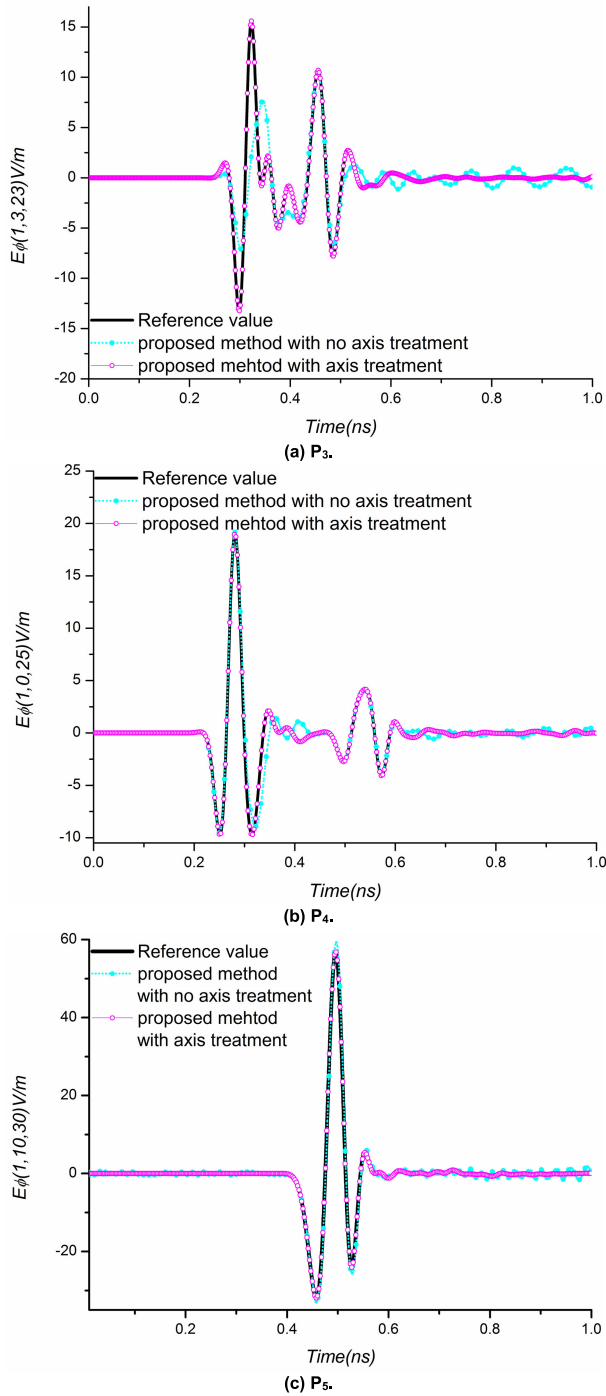


**FIGURE 9.** Waveform results with and without special treatment for on z-axis are compared: (a) P<sub>3</sub>; (b) P<sub>4</sub>; (c) P<sub>5</sub>.

coordinate FDTD method is calculated in large space and used as a reference value for comparison. As shown in Figure (9a) to Figure (9c), they have shown the differences of whether special treatment for on z-axis are performed at the observation points with different intensity of field transformation, It is clear that the special treatment for on z-axis of FDTD method in the 3-D cylindrical coordinate system is very important.

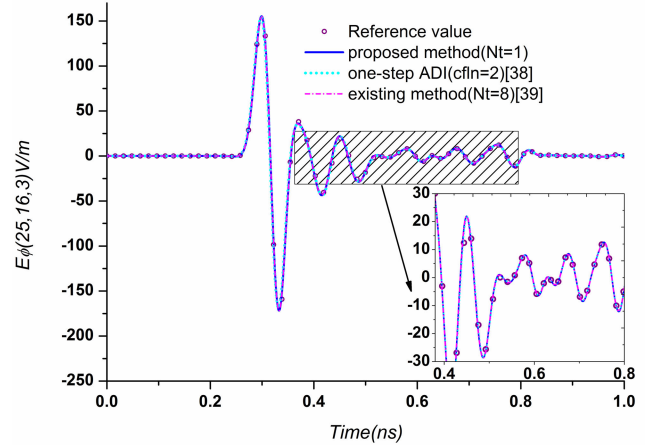


**FIGURE 10.** Waveforms at P<sub>6</sub> of three methods compared with the reference value.

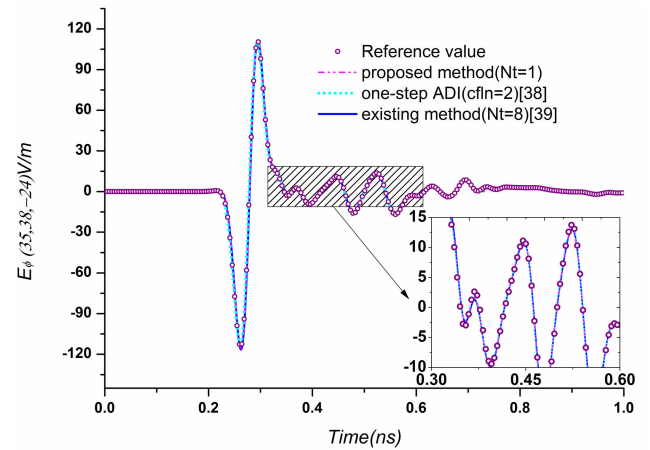


**FIGURE 11.** Waveforms at P<sub>7</sub> of three methods compared with the reference value.

In the third example, in order to verify the advantages of the proposed method in the term of computational efficiency and accuracy, two other observation points are given as P<sub>6</sub>(25, 16, 3) and P<sub>7</sub>(35, 38, -24). The iteration of the computational domain is denoted by Nt, here, as in the second example, the conventional FDTD method in 3-D cylindrical coordinate system is still calculated in large space and used as a reference value for comparison.

As shown in Figure 10 and Figure 11, the reference value, the one-step ADI-FDTD method [38], the existing method [39](calculated in 3-D case) and the proposed method can be used to show the time-domain field waveforms, the numerical results show excellent agreement between the proposed method and the reference value.

In addition, to demonstrate the advantage of the proposed method in accuracy, two error formulations are given, they are defined as

$$E_{\phi-error}(t) = E_{\phi}(t) - E_{\phi-ref}(t)(V/m) \quad (59a)$$

$$E_{\phi-error}(t) = \frac{|E_{\phi}(t) - E_{\phi-ref}(t)|}{|E_{\phi-refmax}(t)|}(\%) \quad (59b)$$



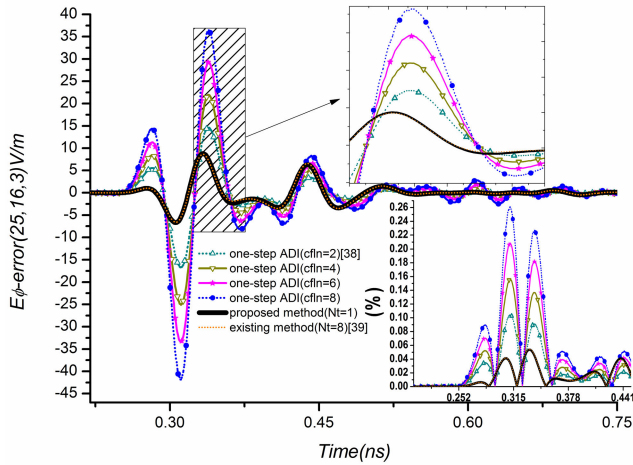


FIGURE 12. Errors at  $P_6$  of three methods with different computational conditions.

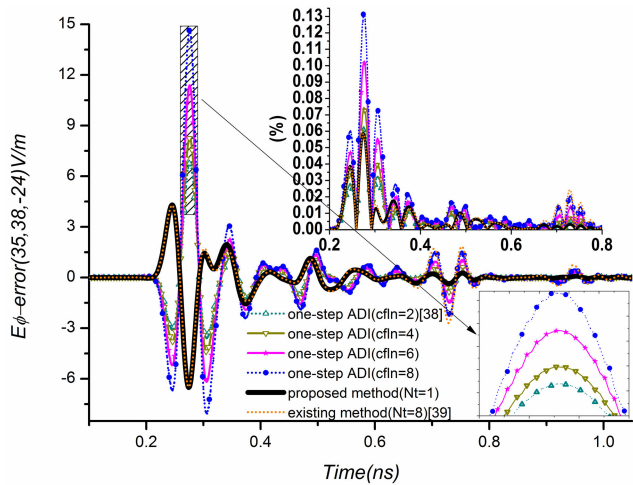


FIGURE 13. Errors at  $P_7$  of three methods with different computational conditions.

where  $E_\phi(t)$  are the simulation datum of the one-step ADI-FDTD method [38], the existing method [39] and the proposed method,  $E_{\phi-ref_{max}}(t)$  is the simulation data of the conventional FDTD calculated with large space.

Figure 12 and Figure 13 give the errors obtained by  $E_\phi$  of the one-step ADI method (cfln=2 - 8) [38], the existing method (Nt = 8) [39] and the proposed method (Nt = 1), and they show that the errors of the existing method and the proposed method are at same level. Even so, in Figure 12, when the Nt of the proposed method is equal to one, its accuracy is 48% higher than that of one-step ADI method when cfln = 2, and 65%, 74% and 79% higher than that of cfln = 4, 6 and 8, respectively. Similarly, as shown in Figure 13, the proposed method also has a greater accuracy advantage over the one-step ADI method.

Table 1 shows the CPU times and memories of four methods with different computational conditions. Obviously, LU decomposition [45] can be programmed to significantly

TABLE 1. Simulation results for the different methods.

	Time step(n)/Order(q)	cfln/Nt	CPU Time(s)	Memory (M)
conventional FDTD	$n=18000$	cfln=1	914	133.9
one-step ADI method [38]	$n=9000$	cfln=2	758	151.5
	4500	4	607	151.5
	3000	6	409	151.4
	2250	8	304	151.5
existing method [39]	$q=170$	Nt=8	467	257.6
proposed method	$q=170$	Nt=1	230	154.1

reduce the memory consumption associated with WLP. Moreover, compared with the existing method (Nt = 8) [39], the computational efficiency of the proposed method (Nt = 1) is improved by 51%. While compared with the one-step ADI method [38], when cfln = 2, 4, 6 and 8, the computational efficiencies of the proposed method can be improved by 70%, 62%, 44% and 24%, respectively. Meanwhile, compared with the conventional FDTD method, the proposed method can improve the time step of the conventional FDTD method by almost four times.

In the fourth example, to validate the performance of the PML implementation of the proposed method, the scattering model as shown in Figure 7 is calculated again. The overall computational domain contains  $50(\rho) \times 40(\phi) \times 90(z)$  cells, and it includes a 10-layer PML in each direction. Moreover, the other conditions are the same as the above examples. Within the PML region, the parameters are scaled using the polynomial profile, which are given elsewhere [50].

$$\sigma_\zeta = \sigma_{\max} \frac{(\zeta - \zeta_0)^m}{d^p} \quad (60a)$$

$$\kappa_\zeta = 1 + \kappa_{\max} \frac{(\zeta - \zeta_0)^m}{d^p}, \quad \zeta = \rho, \phi, z \quad (60b)$$

where  $\zeta_0$  is the location of the interface between the PML region and the inner non-PML region,  $d = 10\Delta\rho = 10\Delta z = 10\Delta$  is the thickness of the PML, and  $\kappa_{\max} = 3$ . In order to minimize reflection error, the best choice of  $\sigma_{\max}$  depends on

$$\sigma_{\max} = \lambda\sigma_{opt} = \frac{\lambda(m+1)}{150\pi\Delta z}. \quad (61)$$

To validate the proposed method, the relative reflection error as a function of time is used and defined as

$$\text{error} = 20\log_{10} \frac{|E_{\phi,PML}(t) - E_{\phi,ref}(t)|}{|E_{\phi,ref_{max}}(t)|} \text{ (dB)} \quad (62)$$

where  $E_{\phi,PML}(t)$  is calculated in the test domain, and  $E_{\phi,ref_{max}}(t)$  has the same meaning as Eq. (59).

The observation point of the reflection error is usually the corner point, so let's take  $P_8$  (25, 0, 25) here. Figure 14 shows the relative reflection errors of the proposed PML absorbing boundary condition under different  $m$ . Obviously, when  $\lambda = 0.9$  and  $m = 4$ , the proposed PML absorbing boundary condition is better than that in the other situations.

As can be seen from Figure 15, when  $d = 10$  cm, the maximum relative reflection errors of the PML absorption



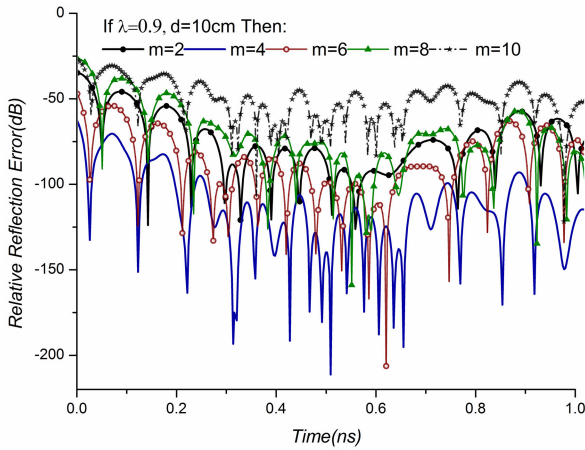


FIGURE 14. Relative reflection errors of the proposed PML implementation under different  $m$  at  $P_8$ .

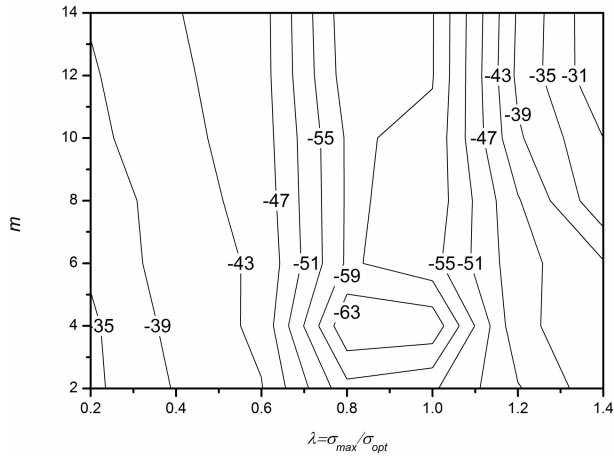


FIGURE 15. Maximum relative reflection errors of different  $m$  and  $\lambda$  at observation point  $P_8$ .

boundary condition at the observation point  $P_8$  can be influenced by the parameters  $m$  and  $\lambda$ . It can be seen that when  $3 \leq m \leq 5$  and  $0.8 \leq \lambda \leq 1.0$ , the relative reflection error of the PML absorption boundary condition of the proposed method can be reduced to about  $-63$  dB.

In the fifth example, to prove the research significance of the proposed method, a numerical example is a cylindrical cavity with a dielectric filling with  $\epsilon_r = 35.74$ . The physical dimensions of the structure is shown in Figure 16. A uniform mesh with  $\Delta\rho = 0.17272$  mm,  $\Delta z = 0.1524$  mm, and the total mesh dimension is  $75(\Delta\rho) \times 40(\Delta\phi = \frac{2\pi}{40}) \times 100(\Delta z)$ . excitation pulse is a Gaussian pulse, where  $t_0 = 0.6$  ns,  $\tau_0 = 0.2$  ns. Figure 17 and Table 2 show the calculation results of  $TM_{01}$  mode. Obviously, when the proposed method takes  $Nt = 1, 2, 4, 8$ , it can still obtain higher calculation accuracy, and when  $Nt=4$ , the efficiency of the proposed method is almost same as that of the conventional FDTD method.

In the sixth example, to further prove the significance of the proposed method, a numerical example of left-handed material [53] is provided here.

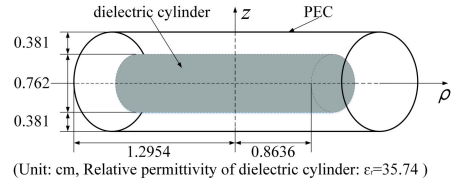


FIGURE 16. Sizes of dielectric cylinder resonator.

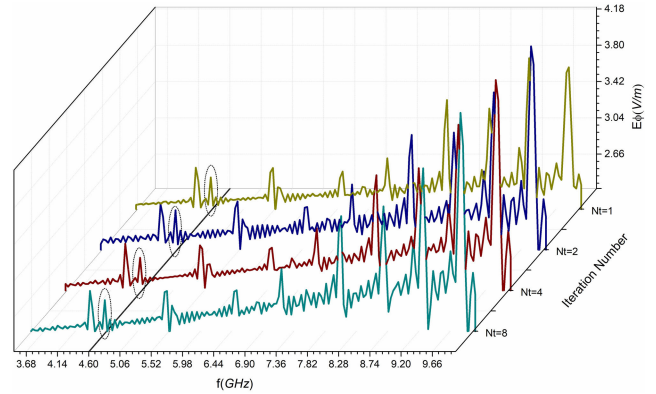


FIGURE 17. Frequency spectrum diagram of  $E_\phi$  of  $TM_{01}$  mode.

TABLE 2. The calculation results of  $TM_{01}$  mode.

	Time step(n)/ Order(q)	cfln/Nt	CPU Time(s)	Results (GHz)	Relative Error (%)
conventional FDTD	$n=60000$	cfln=1	117	4.619	0.4%
proposed method	$q=500$	$Nt=1$	85	4.578	-0.5%
	500	2	104	4.578	-0.5%
	500	4	138	4.578	-0.5%
	500	8	199	4.578	-0.5%

(The theoretical value is 4.60 GHz [52])

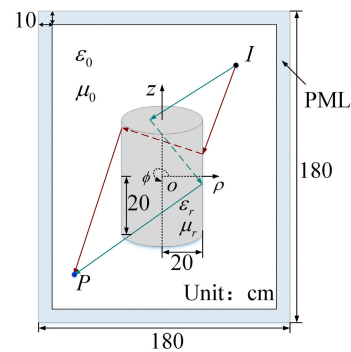
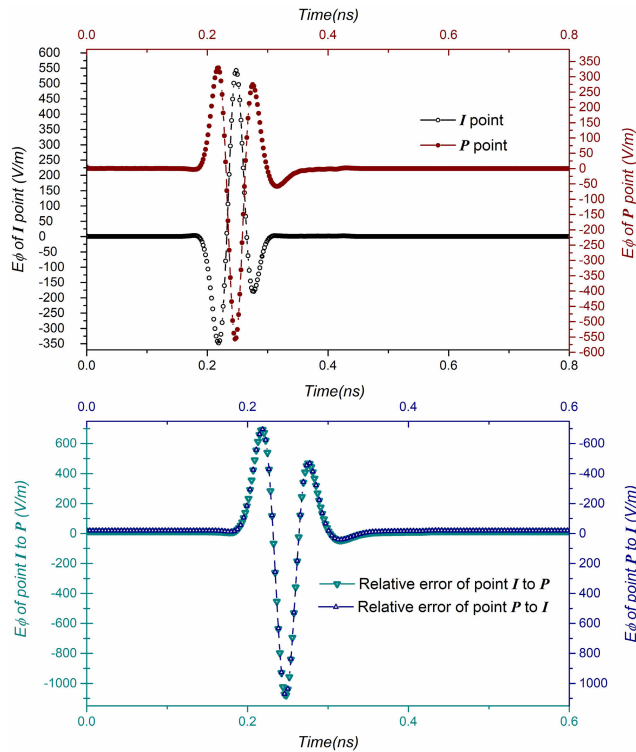
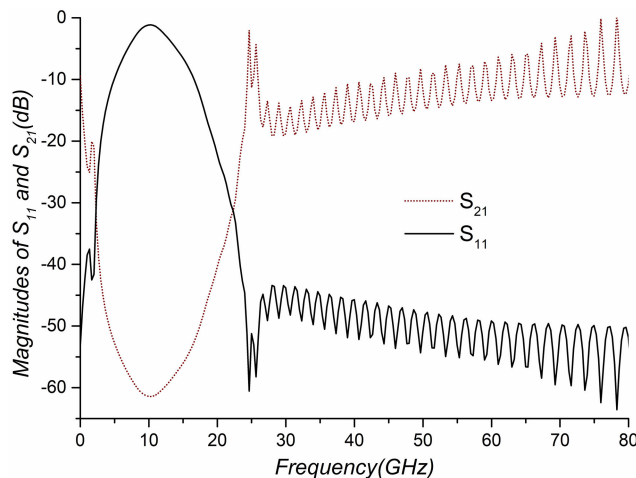


FIGURE 18. The space calculation area of the left-handed material cylinder.

The spatial calculation area and the sizes of the left-handed material cylinder are shown in Figure 18. The electromagnetic wave is absorbed by the PML absorption boundary around the calculation area, the thickness of the PML layer is 10 cm, and the uniform grids are same as the first example. When the excitation source shown in Eq. (48) is added at point



**FIGURE 19.** The negative refraction effect of the proposed method in the left-handed material cylinder.



**FIGURE 20.** Frequency response for the proposed method in the left-handed material cylinder.

I (30, 0, 30), the equivalent permittivity and permeability of the left-handed material cylinder are  $\epsilon_r = -1$  and  $\mu_r = -1$ , respectively. The simulation process shows that the excitation source is refracted from the I point ( $\epsilon_0$  and  $\mu_0$ ) through the left-handed material ( $\epsilon_r$  and  $\mu_r$ ) cylinder, and then imaged again at the P (30, 20, -30) point ( $\epsilon_0$  and  $\mu_0$ ).

As can be seen from Figure 19, the proposed method better demonstrates the lossless negative refraction characteristic of the left-handed material, so that the results at the I and P

points are almost opposite. Meanwhile, the S-parameter spectrum shown in Figure 20 shows that the frequency response of the proposed method in the left-handed material is expected to be around 10 GHz, which is close to the frequency of the incident excitation source.

### VIII. CONCLUSION

In this work, an improved ADI iterative algorithm with Gauss-Seidel ideology for efficient WLP-FDTD method is proposed in 3-D cylindrical coordinate system. Through the existing scheme, it can be seen that the perturbation term and one-step Gauss-Seidel procedure are used to well solve the huge large sparse matrix problem of conventional WLP-FDTD in 3-D cylindrical coordinate system. However, the introduction of the perturbation term will still lead to some splitting errors, so it has to use multiple iterations to reduce the errors. In order to solve the problems, the proposed method uses the characteristics of ADI algorithm to form the ADI linear iterative equations based on the WLP technique, and uses two-step Gauss-Seidel procedures to weaken the influence of the perturbation term in the existing scheme. Numerical examples show that the correction term added by the proposed method can better connect the two-step Gauss-Seidel procedures, which makes the proposed method stable and fast in convergence. In other words, only once iteration of the proposed method can achieve the accuracy of the existing method in eight times iterations. And, the efficiency will be greatly improved. At the same time, there are similar advantages in comparison with the one-step ADI method. Moreover, the proposed method compares with the conventional FDTD method, the efficiency can increase four times step. The PML implementation of the proposed method also shows that the proposed method has certain advantage in accuracy. In addition, the applications of the proposed method in the simulations of dielectric cavity cylinder and left-handed material cylinder can verify the research significance of the proposed method again. Theoretical analysis and several examples prove that the proposed method has obvious improvement compared with previous methods, and can also solve the special structural problems of FDTD method that require special treatment of FDTD differential fields on z-axis and  $\phi$ -direction under 3-D cylindrical coordinate system.

### APPENDIX A

In this appendix, Eq. (1) will be derived.

According to the discussion in [48], the basic equations of FDTD in 3-D cylindrical coordinate system are

$$\frac{\partial e_\rho}{\partial t} = \frac{1}{\epsilon} \left( \frac{1}{\rho} \partial \phi h_z - \partial z h_\phi \right) - \frac{1}{\epsilon} J_{e\rho} \quad (A.1.a)$$

$$\frac{\partial e_\phi}{\partial t} = \frac{1}{\epsilon} (\partial z h_\rho - \partial \rho h_z) - \frac{1}{\epsilon} J_{e\phi} \quad (A.1.b)$$

$$\frac{\partial e_z}{\partial t} = \frac{1}{\epsilon} \left( \frac{1}{\rho} \partial \rho (\rho h_\phi) - \frac{1}{\rho} \partial \phi h_\rho \right) - \frac{1}{\epsilon} J_{ez} \quad (A.1.c)$$

$$\frac{\partial h_\rho}{\partial t} = -\frac{1}{\mu} \left( \frac{1}{\rho} \partial \phi e_z - \partial z e_\phi \right) + \frac{1}{\mu} M_{h\rho} \quad (A.1.d)$$

$$\frac{\partial h_\phi}{\partial t} = -\frac{1}{\mu} (\partial_z e_\rho - \partial_\rho e_z) + \frac{1}{\mu} M_{h\phi} \quad (\text{A.1.e})$$

$$\frac{\partial h_z}{\partial t} = -\frac{1}{\mu} \left( \frac{1}{\rho} \partial_\rho (\rho e_\phi) - \frac{1}{\rho} \partial_\phi e_\rho \right) + \frac{1}{\mu} M_{hz} \quad (\text{A.1.f})$$

For example, we use Eq. (53) to expand Eq. (A.1.a),  $\frac{\partial e_\rho}{\partial t}$  can be expanded as

$$e_\rho^q + 2 \sum e_\rho^\vartheta. \quad (\text{A.2})$$

Therefore, the basic equations of WLP-FDTD in 3-D cylindrical coordinate system can be obtained as follows

$$e_\rho^q + 2 \sum e_\rho^\vartheta = a \left( \frac{1}{\rho} \partial_\phi h_z^q - \partial_z h_\phi^q - J_{e\rho}^q \right) \quad (\text{A.3.a})$$

$$e_\phi^q + 2 \sum e_\phi^\vartheta = a \left( \partial_z h_\rho^q - \partial_\rho h_z^q - J_{e\phi}^q \right) \quad (\text{A.3.b})$$

$$e_z^q + 2 \sum e_z^\vartheta = a \left( \frac{1}{\rho} \frac{\partial(\rho h_\phi^q)}{\partial \rho} - \frac{1}{\rho} \partial_\phi h_\rho^q - J_{ez}^q \right) \quad (\text{A.3.c})$$

$$h_\rho^q + 2 \sum h_\rho^\vartheta = b \left( \partial_z e_\phi^q - \frac{1}{\rho} \partial_\phi e_z^q + M_{h\rho}^q \right) \quad (\text{A.3.d})$$

$$h_\phi^q + 2 \sum h_\phi^\vartheta = b \left( \partial_\rho e_z^q - \partial_z e_\rho^q + M_{h\phi}^q \right) \quad (\text{A.3.e})$$

$$h_z^q + 2 \sum h_z^\vartheta = b \left( \frac{1}{\rho} \partial_\phi e_\rho^q - \frac{1}{\rho} \frac{\partial(\rho e_\phi^q)}{\partial \rho} + M_{hz}^q \right). \quad (\text{A.3.f})$$

where  $a$  and  $b$  are same as Eq. (1), substituting the coefficient matrices into Eq. (1), the group of Eq. (A.3.a)-Eq. (A.3.f) can

be written as matrix multiplication.

$$\begin{bmatrix} \mathbf{W}_E^q \\ \mathbf{W}_H^q \end{bmatrix} - \begin{bmatrix} \mathbf{V}_E^{q-1} \\ \mathbf{V}_H^{q-1} \end{bmatrix} = \begin{bmatrix} 0 & \mathbf{A}_{\mu\chi} + \mathbf{B}_{\mu\chi} \\ \mathbf{A}_{\varepsilon\chi} + \mathbf{B}_{\varepsilon\chi} & 0 \end{bmatrix} \begin{bmatrix} \mathbf{W}_E^q \\ \mathbf{W}_H^q \end{bmatrix} + \begin{bmatrix} \mathbf{R}_J^q \\ \mathbf{R}_M^q \end{bmatrix} \quad (\text{A.4.a})$$

that is

$$\mathbf{W}^q - \mathbf{V}^{q-1} = (\mathbf{A} + \mathbf{B})\mathbf{W}^q + \mathbf{R}_{JM}^q. \quad (\text{A.4.b})$$

Furthermore, Eq. (1) can be obtained by transforming the form of Eq. (A.4.b).

**APPENDIX B**

Because the formulas of the first-order central difference expansions in the proposed method is huge and complex, so, we only take some operation terms to explain.

Eq. (B.1.a) has shown that how to obtain the  $e_{\phi,p+1}^{*q}$  term of Eq. (11a-2) by using first-order central difference as in (B.1.a), shown at the bottom of the page.

Taking  $e_{z,p+1}^q$  and  $e_{\phi,p+1}^q$  of Eq. (13a-1) and Eq. (13a-3) as another examples, their expansions are, (B.1.b) and (B.1.c), as shown at the bottom of the page.

It must be explained that, in Eq. (B.1.c), the spatial position of  $e_{\phi,p+1}^q$  in the  $\phi$ -direction must be same as the spatial position of  $e_{\rho,p+1}^q$  in Eq. (13a-3) before it is expanded in the  $\phi$ -direction.

$$\begin{aligned} ab\partial\rho\left(\frac{1}{\rho}(\partial\rho)\rho\right)e_{\phi,p+1}^{*q} &= ab\partial\rho \left\{ \frac{1}{(i+\frac{1}{2})\Delta\rho} \begin{bmatrix} (i+1)e_{\phi,p+1}^{*q}(i+1, j+\frac{1}{2}, k) \\ -ie_{\phi,p+1}^{*q}(i, j+\frac{1}{2}, k) \end{bmatrix} \right\} \\ &= \frac{ab}{\Delta\rho^2} \left\{ \frac{1}{(i+\frac{1}{2})} \begin{bmatrix} (i+1)e_{\phi,p+1}^{*q}(i+1, j+\frac{1}{2}, k) - ie_{\phi,p+1}^{*q}(i, j+\frac{1}{2}, k) \\ -\frac{1}{(i-\frac{1}{2})} \begin{bmatrix} ie_{\phi,p+1}^{*q}(i, j+\frac{1}{2}, k) - (i-1)e_{\phi,p+1}^{*q}(i-1, j+\frac{1}{2}, k) \end{bmatrix} \end{bmatrix} \right\} \quad (\text{B.1.a}) \end{aligned}$$

$$\begin{aligned} ab\left(\frac{1}{\rho}(\partial\rho)\rho\right)\partial\rho e_{z,p+1}^q &= \frac{ab}{\Delta\rho} \left(\frac{1}{\rho}(\partial\rho)\rho\right) \left\{ e_{z,p+1}^q(i+1, j, k+\frac{1}{2}) - e_{z,p+1}^q(i, j, k+\frac{1}{2}) \right\} \\ &= \frac{ab}{i\Delta\rho^2} \left\{ (i+\frac{1}{2}) \begin{bmatrix} e_{z,p+1}^q(i+1, j, k+\frac{1}{2}) - e_{z,p+1}^q(i, j, k+\frac{1}{2}) \\ -(i-\frac{1}{2}) \begin{bmatrix} e_{z,p+1}^q(i, j, k+\frac{1}{2}) - e_{z,p+1}^q(i-1, j, k+\frac{1}{2}) \end{bmatrix} \end{bmatrix} \right\} \quad (\text{B.1.b}) \end{aligned}$$

$$\begin{aligned} \left(\frac{1}{\rho}(\partial\phi)\right)\left(\frac{1}{\rho}(\partial\rho)\rho\right)e_{\phi,p+1}^q &= ab\frac{1}{\rho}(\partial\phi)\frac{1}{(i+\frac{1}{2})\Delta\rho} \left\{ \begin{bmatrix} (i+1)e_{\phi,p+1}^q(i+1, j, k) \\ -ie_{\phi,p+1}^q(i, j, k) \end{bmatrix} \right\} \\ &= \frac{ab}{(i+\frac{1}{2})^2\Delta\rho^2\Delta\phi} \left\{ \begin{bmatrix} (i+1)e_{\phi,p+1}^q(i+1, j+\frac{1}{2}, k) \\ -(i+1)e_{\phi,p+1}^q(i+1, j-\frac{1}{2}, k) \\ ie_{\phi,p+1}^q(i, j+\frac{1}{2}, k) \\ -ie_{\phi,p+1}^q(i, j-\frac{1}{2}, k) \end{bmatrix} \right\}. \quad (\text{B.1.c}) \end{aligned}$$

## APPENDIX C

In this appendix, the detailed methods for obtaining Eq. (51a) to Eq. (51c) are explained.

Here, Eq. (49a) and Eq. (49b) are taken as examples to explain, seeing the  $\frac{\partial E_\rho}{\partial \bar{z}}$  term of Eq. (49b), we can find that the derivative of the field with respect to  $\bar{z}$  can be written as

$$\frac{\partial \rho}{\partial \bar{z}} = \frac{\partial \rho}{\partial z} \cdot \frac{\partial z}{\partial \bar{z}}. \quad (\text{C.1.a})$$

Obviously, we can get from (50b)

$$\frac{\partial \bar{z}}{\partial z} = \xi_z(z) = \xi_z. \quad (\text{C.1.b})$$

Substituting Eq. (C.1.b) into Eq. (C.1.a), we can obtain

$$\frac{\partial \rho}{\partial \bar{z}} = \frac{1}{\xi_z} \frac{\partial \rho}{\partial z}. \quad (\text{C.1.c})$$

Similarly, seeing the  $\frac{\partial E_z}{\partial \bar{\rho}}$  term of Eq. (49b), we also can find that the derivative of the field with respect to  $\bar{\rho}$  can be written as

$$\frac{\partial z}{\partial \bar{\rho}} = \frac{\partial z}{\partial \rho} \cdot \frac{\partial \rho}{\partial \bar{\rho}}. \quad (\text{C.2.a})$$

The derivative of Eq. (50a) is obtained as

$$\frac{\partial \bar{\rho}}{\partial \rho} = \xi_\rho(\rho) = \xi_\rho. \quad (\text{C.2.b})$$

Substituting Eq. (C.2.b) into Eq. (C.2.a), we can obtain

$$\frac{\partial z}{\partial \bar{\rho}} = \frac{1}{\xi_\rho} \frac{\partial z}{\partial \rho}. \quad (\text{C.2.c})$$

Clearly, we substitute Eq. (C.1.c) and Eq. (C.2.c) into Eq. (49b), Eq. (52b) is formed.

Next, let's define

$$\frac{\bar{\rho}}{\rho} = \xi_\phi(\rho) = \xi_\phi. \quad (\text{C.3.a})$$

Therefore, the  $\frac{1}{\bar{\rho}} \frac{\partial E_z}{\partial \bar{\phi}}$  term of Eq. (49a) can be written as

$$\frac{\rho}{\bar{\rho}} \frac{1}{\rho} \frac{\partial E_z}{\partial \bar{\phi}} = \frac{1}{\rho} \frac{1}{\xi_\phi} \frac{\partial E_z}{\partial \phi}. \quad (\text{C.3.b})$$

Clearly, we substitute Eq. (C.1.b) and Eq. (C.3.b) into Eq. (49a), Eq. (52a) is formed.

## APPENDIX D

In this appendix, the detailed derivation processes from Eq. (52) to Eq. (57) are shown.

Here, Eq. (52c) and Eq. (52f) are taken as examples to derive.

According to Eq. (54), we can expand Eq. (52c) and Eq. (52f) by using the splitting field technique as

$$\kappa_\rho \frac{\partial h_{z\rho}}{\partial t} + \frac{\sigma_\rho}{\varepsilon_0} h_{z\rho} = -\frac{1}{\mu} \frac{\partial e_\phi}{\partial \rho} + \frac{1}{\mu} \xi_\rho M_{z\rho} \quad (\text{D.1.a1})$$

$$\kappa_\phi \frac{\partial h_{z\phi}}{\partial t} + \frac{\sigma_\phi}{\varepsilon_0} h_{z\phi} = -\frac{1}{\mu} \frac{1}{\rho} \left( e_\phi - \frac{\partial e_\rho}{\partial \phi} \right) + \frac{1}{\mu} \xi_\phi M_{z\phi} \quad (\text{D.1.a2})$$

$$\kappa_\rho \frac{\partial e_{z\rho}}{\partial t} + \frac{\sigma_\rho}{\varepsilon_0} e_{z\rho} = \frac{1}{\varepsilon} \frac{\partial h_\phi}{\partial \rho} - \frac{1}{\varepsilon} \xi_\rho J_{z\rho} \quad (\text{D.2.a1})$$

$$\kappa_\phi \frac{\partial e_{z\phi}}{\partial t} + \frac{\sigma_\phi}{\varepsilon_0} e_{z\phi} = \frac{1}{\varepsilon} \frac{1}{\rho} \left( h_\phi - \frac{\partial h_\rho}{\partial \phi} \right) - \frac{1}{\varepsilon} \xi_\phi J_{z\phi} \quad (\text{D.2.a2})$$

in which, Eq. (D.1.a1) and Eq. (D.1.a2) are the two sub-items of Eq. (52c) after using the splitting field technique. Similarly, Eq. (D.2.a1) and Eq. (D.2.a2) are the sub-items of Eq. (52f).

According to Eq. (A.2), we can directly obtain the Laguerre equations of Eq. (D.1.a1)-Eq. (D.2.a2) as

$$h_{z\rho}^q = \left( 1 + \frac{2\sigma_\rho}{\kappa_\rho s \varepsilon_0} \right)^{-1} \times \left( -\frac{1}{\kappa_\rho} \frac{2}{s \mu} \partial \rho e_\phi^q - 2 \sum h_{z\rho}^\vartheta + \frac{\xi_\rho}{\kappa_\rho} \frac{2}{s \mu} M_{z\rho}^q \right) \quad (\text{D.3.a1})$$

$$h_{z\phi}^q = \left( 1 + \frac{2\sigma_\phi}{\kappa_\phi s \varepsilon_0} \right)^{-1} \times \left( -\frac{1}{\kappa_\phi} \frac{2}{s \mu} \frac{1}{\rho} \left( e_\phi^q - \partial \phi e_\rho^q \right) - 2 \sum h_{z\phi}^\vartheta + \frac{\xi_\phi}{\kappa_\phi} \frac{2}{s \mu} M_{z\phi}^q \right) \quad (\text{D.3.a2})$$

$$e_{z\rho}^q = \left( 1 + \frac{2\sigma_\rho}{\kappa_\rho s \varepsilon_0} \right)^{-1} \times \left( \frac{1}{\kappa_\rho} \frac{2}{s \varepsilon} \partial \rho h_\phi^q - 2 \sum e_{z\rho}^\vartheta - \frac{\xi_\rho}{\kappa_\rho} \frac{2}{s \varepsilon} J_{z\rho}^q \right) \quad (\text{D.4.a1})$$

$$e_{z\phi}^q = \left( 1 + \frac{2\sigma_\phi}{\kappa_\phi s \varepsilon_0} \right)^{-1} \times \left( \frac{1}{\kappa_\phi} \frac{2}{s \varepsilon} \frac{1}{\rho} \left( h_\phi^q - \partial \phi h_\rho^q \right) - 2 \sum e_{z\phi}^\vartheta + \frac{\xi_\phi}{\kappa_\phi} \frac{2}{s \varepsilon} J_{z\phi}^q \right). \quad (\text{D.4.a2})$$

We combine Eq. (D.3.a1) and Eq. (D.3.a2), and Eq. (56c) is formed, the Eq. (56f) is formed similarly.

## REFERENCES

- [1] A. Taflov and S. C. Hangess, "Introduction to Maxwell's equations and the Yee algorithm," in *Computational Electrodynamics: The Finite-Difference Time-Domain Method*, 2nd ed. Boston, MA, USA: Artech House, 1995, ch. 3, pp. 67–106.
- [2] M. Fusco, "FDTD algorithm in curvilinear coordinates (EM scattering)," *IEEE Trans. Antennas Propag.*, vol. 38, no. 1, pp. 76–89, Jan. 1990.
- [3] W. J. Buchanan, N. K. Gupta, and M. Arnold, "Simulation of radiation from a microstrip antenna using three-dimensional finite-difference time-domain (FDTD) method," in *Proc. 8th Int. Conf. Antennas Propag.*, 1993, pp. 639–642.
- [4] K. S. Yee, J. S. Chen, and A. H. Chang, "Conformal finite difference time domain (FDTD) with overlapping grids," *IEEE Trans. Antennas Propag.*, vol. 40, no. 9, pp. 1068–1075, Sep. 1992.
- [5] A. C. Cangellaris, "Numerical stability and numerical dispersion of a compact 2-D/FDTD method used for the dispersion analysis of waveguides," *IEEE Microw. Guided Wave Lett.*, vol. 3, no. 1, pp. 3–5, Jan. 1993.
- [6] R. Luebbers and C. Penney, "Scattering from apertures in ground planes using FDTD," in *Proc. IEEE Antennas Propag. Soc. Int. Symp.*, Jun. 1993, pp. 822–825.
- [7] Y. E. Erdemli and J. L. Yolakis, "FDTD scattering analysis of cavities with dielectric protrusions," in *Proc. IEEE Antennas Propag. Soc. Int. Symp.*, Jul. 1996, pp. 1660–1663.
- [8] K. S. Yee, J. S. Chen, and A. H. Chang, "Numerical experiments on PEC boundary condition and late time growth involving the FDTD/FDTD and FDTD/FVTD hybrid," in *Proc. IEEE Antennas Propag. Soc. Int. Symp.*, Jun. 1995, pp. 624–627.



- [9] Q. H. Lin, "PML-FDTD method for elastic waves in cylindrical and spherical coordinates," in *IEEE Antennas Propag. Soc. Int. Symp., Dig. Held Conjoint USNC/URSI Nat. Radio Sci. Meeting*, Jul. 1999, pp. 1392–1395.
- [10] A. Munir, "Computational approach for resonant frequency calculation of coaxial cavity resonator using cylindrical coordinate system-based FDTD method," in *Proc. Int. Conf. Quality Res. (QiR)*, Bandung, Indonesia, Aug. 2015, pp. 73–76.
- [11] Y. Taniguchi, Y. Baba, N. Nagaoka, and A. Ametani, "Representation of an arbitrary-radius wire for FDTD calculations in the 2-D cylindrical coordinate system," *IEEE Trans. Electromagn. Compat.*, vol. 50, no. 4, pp. 1014–1018, Nov. 2008.
- [12] A. D. Setiawan, H. Nusantara, and A. Munir, "Resonant frequency computation of dielectric material loaded circular waveguide using cylindrical coordinate system-based FDTD method," in *Proc. Int. Conf. Electr. Eng. Informat. (ICEEI)*, Aug. 2015, pp. 314–317.
- [13] M. Andreasen, "Scattering from bodies of revolution," *IEEE Trans. Antennas Propag.*, vol. AP-13, no. 2, pp. 303–310, Mar. 1965.
- [14] A. Trakic, H. Wang, F. Liu, H. S. Lopez, and S. Crozier, "Analysis of transient eddy currents in MRI using a cylindrical FDTD method," *IEEE Trans. Appl. Supercond.*, vol. 16, no. 3, pp. 1924–1936, Sep. 2006.
- [15] D. B. Davidson and R. W. Ziolkowski, "Body-of-revolution finite-difference time-domain modeling of space-time focusing by a three-dimensional lens," *J. Opt. Soc. Amer. A, Opt. Image Sci.*, vol. 11, no. 4, pp. 1471–1490, Apr. 1994.
- [16] M. J. M. van der Vorst and P. J. I. de Maagt, "Efficient body of revolution finite-difference time-domain modeling of integrated lens antennas," *IEEE Microw. Wireless Compon. Lett.*, vol. 12, no. 7, pp. 258–260, Jul. 2002.
- [17] B. Chen, H. Chen, and B. Zhou, "Analysis of wave propagation in circular tunnel using BOR-FDTD method," in *Proc. IEEE Int. Symp. Microw. Antenna, Propag. EMC Technol. Wireless Commun.*, Aug. 2005, pp. 108–111.
- [18] H. L. Chen, B. Chen, and F. H. Guan, "BOR-FDTD algorithm for propagating obliquely incident pulsed plane wave," *Chin. J. Radio Sci.*, vol. 22, no. 4, pp. 680–684, Aug. 2007.
- [19] F. H. Guan, B. Chen, H. Chen, D. Fang, W. Yu, and L. Zhang, "FDTD method for electromagnetic scattering by body of revolution with obliquely incident pulse plane wave," *Chin. J. Comput. Phys.*, vol. 24, no. 3, pp. 347–352, May 2007.
- [20] C. Bin, D. Yantao, C. Hailin, Z. Bihua, G. Cheng, and S. Lihua, "Study on UWB and HPM propagation in circular tunnel using BOR-FDTD method," in *Proc. 4th Asia-Pacific Conf. Environ. Electromagn.*, Aug. 2006, pp. 688–691.
- [21] H.-L. Chen, B. Chen, Y. Yi, and D.-G. Fang, "Unconditionally stable ADI-BOR-FDTD algorithm for the analysis of rotationally symmetric geometries," *IEEE Microw. Wireless Compon. Lett.*, vol. 17, no. 4, pp. 304–306, Apr. 2007.
- [22] Y. Wang, B. Chen, H. Chen, and R. Xiong, "An unconditionally stable one-step leapfrog ADI-BOR-FDTD method," *IEEE Antennas Wireless Propag. Lett.*, vol. 12, pp. 647–650, 2013.
- [23] J. Shibayama, B. Murakami, J. Yamauchi, and H. Nakano, "LOD-BOR-FDTD algorithm for efficient analysis of circularly symmetric structures," *IEEE Microw. Wireless Compon. Lett.*, vol. 19, no. 2, pp. 56–58, Feb. 2009.
- [24] Y.-G. Wang, Y. Yi, B. Chen, H.-L. Chen, K. Luo, and R. Xiong, "One-step leapfrog LOD-BOR-FDTD algorithm with CPML implementation," *Int. J. Antennas Propag.*, vol. 2016, pp. 1–8, Jan. 2016.
- [25] J. Shibayama, T. Oikawa, J. Yamauchi, and H. Nakano, "Efficient LOD-BOR-FDTD implementation based on a fundamental scheme," *IEEE Photon. Technol. Lett.*, vol. 24, no. 11, pp. 957–959, Jun. 2012.
- [26] J. Chen and J. Wang, "A novel body-of-revolution finite-difference time-domain method with weakly conditional stability," *IEEE Microw. Wireless Compon. Lett.*, vol. 18, no. 6, pp. 377–379, Jun. 2008.
- [27] Y. Wang, Y. Yi, B. Chen, H. Chen, and K. Luo, "One-step leapfrog weakly conditionally stable finite-difference time-domain method for body of revolution," *IET Microw. Antennas Propag.*, vol. 9, no. 14, pp. 1522–1526, Nov. 2015.
- [28] J. Chen and J. Wang, "The body-of-revolution hybrid implicit-explicit finite-difference time-domain method with large time step size," *IEEE Trans. Electromagn. Compat.*, vol. 50, no. 2, pp. 369–374, May 2008.
- [29] D. W. Zhu, Y. G. Wang, H. L. Chen, and B. Chen, "A one-step leapfrog HIE-FDTD method for rotationally symmetric structures," *Int. J. RF Microw. Comput.-Aided Eng.*, vol. 27, no. 4, pp. 1–7, Jan. 2017.
- [30] H.-L. Chen, B. Chen, Y.-F. Mao, Y. Yi, and B.-H. Zhou, "A memory-efficient formulation of the unconditionally stable WLP-BOR-FDTD method," in *Proc. 8th Int. Symp. Antennas, Propag. EM Theory*, 2008, pp. 748–750.
- [31] H.-L. Chen, B. Chen, Y.-T. Duan, Y. Yi, and D.-G. Fang, "Unconditionally stable Laguerre-based BOR-FDTD scheme for scattering from bodies of revolution," *Microw. Opt. Technol. Lett.*, vol. 49, no. 8, pp. 1897–1900, Aug. 2007.
- [32] D. Zhu, H. Chen, J. Yang, Y. Yi, and B. Chen, "A novel efficient WLP-based BOR FDTD method with explicit treating ideology," *IEEE Access*, vol. 7, pp. 16858–16869, 2019.
- [33] N. Dib, T. Weller, and M. Scardelletti, "Analysis of 3-D cylindrical structures using the finite difference time domain method," in *IEEE MTT-S Int. Microw. Symp. Dig.*, Baltimore, MD, USA, 1998, pp. 925–928.
- [34] Y. Chen, R. Mittra, and P. Harms, "Finite-difference time-domain algorithm for solving Maxwell's equations in rotationally symmetric geometries," *IEEE Trans. Microw. Theory Techn.*, vol. 44, no. 6, pp. 832–839, Jun. 1996.
- [35] Z. Kancleris, "Handling of singularity in finite-difference time-domain procedure for solving Maxwell's equations in cylindrical coordinate system," *IEEE Trans. Antennas Propag.*, vol. 56, no. 2, pp. 610–613, Feb. 2008.
- [36] M. F. Hadi and A. Z. Elsherbeni, "Numerical dispersion and stability for three-dimensional cylindrical FDTD near the axis of rotation," in *Proc. 11th Eur. Conf. Antennas Propag. (EUCAP)*, Paris, France, Mar. 2017, pp. 936–938.
- [37] C. Yuan and Z. Chen, "A three-dimensional unconditionally stable ADI-FDTD method in the cylindrical coordinate system," *IEEE Trans. Microw. Theory Techn.*, vol. 50, no. 10, pp. 2401–2405, Oct. 2002.
- [38] Y. Wang, B. Chen, H. Chen, Y. Yi, and X. Kong, "One-step leapfrog ADI-FDTD method in 3-D cylindrical grids with a CPML implementation," *IEEE Antennas Wireless Propag. Lett.*, vol. 13, pp. 714–717, 2014.
- [39] Y. Wang, Y. Yi, H. Chen, Z. Chen, Y. Duan, and B. Chen, "An efficient Laguerre-based BOR-FDTD method using Gauss-Seidel procedure," *IEEE Trans. Antennas Propag.*, vol. 64, no. 5, pp. 1829–1839, May 2016.
- [40] Y.-S. Chung, T. K. Sarkar, B. Ho Jung, and M. Salazar-Palma, "An unconditionally stable scheme for the finite-difference time-domain method," *IEEE Trans. Microw. Theory Techn.*, vol. 51, no. 3, pp. 697–704, Mar. 2003.
- [41] Z. Chen, Y. Duan, Y. Zhang, H. Chen, and Y. Yi, "A new efficient algorithm for 3-D Laguerre-based finite-difference time-domain method," *IEEE Trans. Antennas Propag.*, vol. 62, no. 4, pp. 2158–2164, Apr. 2014.
- [42] B. Zhang, Y. Yi, Y. Duan, Z. Chen, and B. Chen, "A new iterative algorithm for efficient 3-D Laguerre-based FDTD method," *IEEE Antennas Wireless Propag. Lett.*, vol. 15, pp. 662–665, 2016.
- [43] T. Stefanski and T. D. Drysdale, "Improved implementation of the Mur first-order absorbing boundary condition in the ADI-FDTD method," *Microw. Opt. Technol. Lett.*, vol. 50, no. 7, pp. 1757–1761, Jul. 2008.
- [44] J. Shibayama, M. Ito, J. Yamauchi, and H. Nakano, "A fundamental LOD-FDTD method in cylindrical coordinates," *IEEE Photon. Technol. Lett.*, vol. 29, no. 11, pp. 865–868, Jun. 1, 2017.
- [45] G. H. Golub and C. F. van Loan, "Iterative methods for linear systems," in *Matrix Computation*, 3rd ed. Baltimore, MD, USA: John Hopkins Univ. Press, 1995, ch. 10, pp. 509–544.
- [46] S. H. Weintraub, "Solving systems of linear differential equations," in *Jordan Canonical Form: Application to Differential Equations*. Bethlehem, PA, USA: Lehigh Univ., 2008, ch. 2, pp. 24–53.
- [47] Z. Mei, Y. Zhang, X. Zhao, B. H. Jung, T. K. Sarkar, and M. Salazar-Palma, "Choice of the scaling factor in a marching-on-in-degree time domain technique based on the associated Laguerre functions," *IEEE Trans. Antennas Propag.*, vol. 60, no. 9, pp. 4463–4467, Sep. 2012.
- [48] F. Zhen, Z. Chen, and J. Zhang, "Toward the development of a three-dimensional unconditionally stable finite-difference time-domain method," *IEEE Trans. Microw. Theory Techn.*, vol. 48, no. 9, pp. 1550–1558, Sep. 2000.
- [49] V. E. Nascimento, B.-H.-V. Borges, and F. L. Teixeira, "Split-field PML implementations for the unconditionally stable LOD-FDTD method," *IEEE Microw. Wireless Compon. Lett.*, vol. 16, no. 7, pp. 398–400, Jul. 2006.
- [50] S. Luo and Z. Chen, "A FDTD-based modal PML," *IEEE Microw. Wireless Compon. Lett.*, vol. 16, no. 10, pp. 528–530, Oct. 2006.



[51] G. Mur, "Absorbing boundary conditions for the finite-difference approximation of the time-domain electromagnetic-field equations," *IEEE Trans. Electromagn. Compat.*, vol. EMC-23, no. 4, pp. 377–382, Nov. 1981.

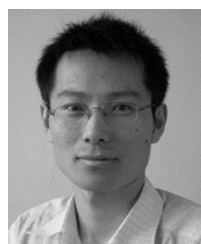
[52] M. M. Taheri and D. Mirshekar-Syahkal, "Accurate determination of modes in dielectric-loaded cylindrical cavities using a one-dimensional finite element method," *IEEE Trans. Microw. Theory Techn.*, vol. 37, no. 10, pp. 1536–1541, Oct. 1989.

[53] J. B. Pendry, "Negative refraction makes a perfect lens," *Phys. Rev. Lett.*, vol. 85, no. 18, pp. 3966–3969, Oct. 2000.



**DA-WEI ZHU** was born in Jilin, China, in 1983. He received the B.S. degree in computer science and technology and the M.S. degree in computer system structure from the Changchun University of Science and Technology, Changchun, China, in 2007 and 2011, respectively, and the Ph.D. degree from the National Key Laboratory on Electromagnetic Environmental Effects and Electro-Optical Engineering, PLA University of Science and Technology, Nanjing, China.

He is currently an Associate Professor with the Nanjing Vocational University of Industry Technology, Nanjing. His research interests include computational electromagnetics, lightning protection, and electromagnetic materials.



**HAI-LIN CHEN** was born in Shandong, China, in 1979. He received the B.S. degree in electrical engineering from Qingdao University, Shandong, in 2001, and the M.S. and Ph.D. degrees in electrical engineering from the Nanjing Engineering Institute, Nanjing, China, in 2004 and 2008, respectively.

He is currently an Associate Professor with the National Key Laboratory on Electromagnetic Environmental Effects and Electro-Optical Engineering, PLA University of Science and Technology, Nanjing. His research interests include computational electromagnetics, lightning protection, and electromagnetic materials.



**JIACHEN XU** received the B.S. degree in electronics and information engineering from the Harbin Institute of Technology, Harbin, China, in 2007, the M.S. degree in internet and mobile communications from the University of York, York, U.K., in 2009, and the Ph.D. degree in material processing engineering from the Nanjing University of Aeronautics and Astronautics, Nanjing, China.

His research interests include microelectronics packaging, new welding processes, and welding materials.



**BO-AO XU** was born in Liaoning, China, in 1989. He received the B.S. degree in physics from the Dalian University of Technology, Dalian, China, in 2012, the M.S. degree in electronic science and technology from the Nanjing Engineering Institute, Nanjing, China, in 2015, and the Ph.D. degree from the National Key Laboratory on Electromagnetic Environmental Effects and Electro-optical Engineering, PLA University of Science and Technology, Nanjing, in 2019. He is currently an

engineer in ROCKET FORCE ACADEMY, Beijing, China. His research interests include computational electromagnetics and EMP.



**LI ZHEN** received the B.Eng. and M.Eng. degrees from Northwestern Polytechnical University, Xi'an, China, in 2002 and 2005, respectively, and the Ph.D. degree in electrical engineering from Nanjing University, Nanjing, China, in 2015.

Since 2017, he has been with the Nanjing Vocational University of Industry Technology, where he is currently an Associate Professor with the School of the Electrical Engineering. His current research interests include electromagnetic metamaterial and microwave circuits.

...